Impact of small-scale disturbances on geochemical conditions, biogeochemical processes and element fluxes in surface sediments of the eastern Clarion-Clipperton Zone, Pacific Ocean

Jessica B. Volz[a,*], Laura Haffert[b], Matthias Haeckel[b], Andrea Koschinsky[c], Sabine Kasten[a,d]

[a] Alfred Wegener Institute Helmholtz Centre for Polar and Marine Research, 27570 Bremerhaven, Germany

[b] GEOMAR Helmholtz Centre for Ocean Research Kiel, 24148 Kiel, Germany

[c] Jacobs University Bremen, Department of Physics and Earth Sciences, 28759 Bremen, Germany

[d] University of Bremen, Faculty of Geosciences, Klagenfurter Strasse, 28359 Bremen, Germany

*Corresponding author:

Tel: +49 471 4831 1842

Email: Jessica.volz@awi.de

Keywords: Deep-sea mining, CCZ, polymetallic nodules, redox zonation, oxygen penetration depth, solid-phase manganese

Abstract

The thriving interest in harvesting deep-sea mineral resources, such as polymetallic nodules, calls for environmental impact studies, and ultimately, for regulations for environmental protection. Industrial-scale deep-sea mining of polymetallic nodules most likely has severe consequences for the natural environment. However, the effects of mining activities on deep-sea ecosystems, sediment geochemistry and element fluxes are still poorly understood. Predicting the environmental impact is challenging due to the scarcity of environmental baseline studies as well as the lack of mining trials with industrial mining equipment in the deep sea. Thus, currently we have to rely on small-scale disturbances simulating deep-sea mining activities as a first-order approximation to study the expected impacts on the abyssal environment.

Here, we investigate surface sediments in disturbance tracks of seven small-scale benthic impact experiments, which have been performed in four European contract areas for the exploration of polymetallic nodules in the Clarion-Clipperton Zone (CCZ). These small-scale disturbance experiments were performed 1 day to 37 years prior to our sampling program in the German, Polish, Belgian and French contract areas using different disturbance devices. We show that the depth distribution of solid-phase Mn in the upper 20 cm of the sediments in the CCZ provides a reliable tool for the determination of the disturbance depth, which has been proposed in a previous study (Paul et al., 2018). We found that the upper 5–15 cm of the sediments were removed during various small-scale disturbance experiments in the different exploration contract areas. Transient transport-reaction modelling for the Polish and German contract areas reveals that the removal of the surface sediments is associated with the loss of reactive labile organic carbon. As a result, oxygen consumption rates decrease significantly after the removal of the surface sediments, and consequently, oxygen penetrates up to tenfold deeper into the sediments inhibiting denitrification and Mn(IV) reduction. Our model results show that the return to steady state geochemical conditions after the disturbance is controlled by diffusion until the reactive labile TOC fraction in the surface sediments is partly re-established and the biogeochemical processes commence. While the re-establishment of bioturbation is essential, steady state geochemical conditions are ultimately controlled by the delivery rate of organic matter to the seafloor. Hence, under current depositional conditions, new steady state geochemical conditions in the sediments of the CCZ is reached only on a millennium-scale even for these small-scale disturbances simulating deep-sea mining activities.

1. Introduction

The accelerating global demand for metals and rare-earth elements are driving the economic interest in deep-sea mining (e.g., Glasby, 2000; Hoagland et al., 2010; Wedding et al., 2015). Seafloor minerals of interest include (1) polymetallic nodules (e.g., Mero, 1965), (2) massive sulfide deposits (e.g., Scott, 1987) and (3) cobalt-rich crusts (e.g., Halkyard, 1985). As the seafloor within the Clarion-Clipperton Zone (CCZ) in the NE Pacific holds one of the most extensive deposits of polymetallic nodules with considerable base metal quantities, commercial exploitation of seafloor mineral deposits may focus on the CCZ (e.g., Mero, 1965; Halbach et al., 1988; Rühlemann et al., 2011; Hein et al., 2013; Kuhn et al., 2017a). The exploration, and ultimately, industrial exploitation of polymetallic nodules demands for international regulations for the protection of the environment (e.g., Halfar and Fujita, 2002; Glover and Smith, 2003; Davies et al., 2007; van Dover, 2011; Ramirez-Llodra et al., 2011; Boetius and Haeckel, 2018). The International Seabed Authority (ISA) is responsible for regulating the exploration and exploitation of marine mineral resources as well as for protecting and conserving the marine environment beyond the exclusive economic zones of littoral states from harmful effects (ISA, 2010). The ISA has granted temporal contracts for the exploration of polymetallic nodules in the CCZ, engaging all contract holders to explore resources, test mining equipment and assess the environmental impacts of deep-sea mining activities (ISA 2010; Lodge et al., 2014; Madureira et al., 2016).

Although a considerable number of environmental impact studies have been conducted in different nodule fields, the prediction of environmental consequences of potential future deep-sea mining is still difficult (e.g., Ramirez-Llodra et al., 2011; Jones et al., 2017; Gollner et al., 2017; Cuvelier et al., 2018). In case of the CCZ, the evaluation of the environmental impact of deep-sea mining activities is challenging due to the fact that baseline data on the natural spatial heterogeneity and temporal variability of depositional conditions, benthic communities and the biogeochemical processes in the sediments are scarce (e.g., Mewes et al., 2014; 2016; Vanreusel et al., 2016; Mogollón et al., 2016; Juan et al., 2018; Volz et al., 2018; Menendez et al., 2018; Hauquier et al., 2019). In addition, there is no clear consensus on the most appropriate mining techniques for the commercial exploitation of nodules, and technical challenges due to the inaccessibility of nodules at great water depths between 4000–5000 m have limited the deployment of deep-sea mining systems until today (e.g., Chung, 2010; Jones et al., 2017).

The physical removal of nodules as hard-substrate habitats has severe consequences for the nodule-associated sessile fauna as well as the mobile fauna (Bluhm, 2001; Smith et al., 2008;

Purser et al., 2016; Vanreusel et al., 2016). With slow nodule growth rates of a few millimeters per million years (e.g., Halbach et al., 1988; Kuhn et al., 2017a), the deep-sea fauna may not recover for millions of years (Vanreusel et al., 2016; Jones et al., 2017; Gollner et al., 2017; Stratmann et al., 2018). In addition to the removal of deep-sea fauna as well as seafloor habitats, the exploitation of nodules is associated with (1) the removal, mixing and re-suspension of the upper 4 cm to more than several tens of centimeters of the sediments, (2) the re-deposition of material from the suspended sediment plume, and (3) potentially also the compaction of the surface sediments due to weight of the nodule collector (Thiel, 2001; Oebius et al., 2001; König et al., 2001; Grupe et al., 2001; Radziejewska, 2002; Khripounoff et al., 2006; Cronan et al., 2010; Paul et al., 2018; Gillard et al., 2019). The wide range of estimates for the disturbance depth may be associated with (1) various devices used for the deep-sea disturbance experiments (Brockett and Richards, 1994; Oebius et al., 2001; Jones et al., 2017), (2) distinct sediment properties in different nodule fields of the Pacific Ocean (e.g., Cronan et al., 2010; Hauquier et al., 2019) as well as (3) different approaches for the determination of the disturbance depth (e.g., Oebius et al., 2001; Grupe et al., 2001; Khripounoff et al., 2006). Based on the observation that bulk solid-phase Mn contents decrease over depth in the surface sediments of the DISCOL area, Paul et al. (2018) have suggested that the depth distribution of solid-phase Mn and associated metals (e.g., Mo, Ni, Co, Cu) could be used to trace the sediment removal by disturbances. In addition, other solid-phase properties such as organic carbon contents (TOC), porosity and radioisotopes may be suitable for the determination of the disturbance depth.

The most reactive TOC compounds, found in the bioturbated uppermost sediment layer, are the main drivers for early diagenetic processes (e.g., Froelich et al., 1979; Berner, 1981) and are expected to be removed during mining activities (König et al., 2001). Thus, strong biogeochemical implications can be expected in the sediments after deep-sea mining activities. König et al. (2001) have applied numerical modelling to study the consequences of the removal of the upper 10 cm of the sediments in the DISCOL area in the Peru Basin. They showed that the degradation of TOC during aerobic respiration, denitrification and Mn(IV) reduction may be decreased for centuries increasing the oxygen penetration depth (OPD).

Here, we investigate the impact of various small-scale disturbances on geochemical conditions, biogeochemical processes and element fluxes in surface sediments of the CCZ. These small-scale disturbance tracks were created up to 37 years ago in four different European contract areas for the exploration of polymetallic nodules, including the German BGR (Bundesanstalt für Geowissenschaften und Rohstoffe) area, the Belgian GSR (Global Sea Mineral Resources NV) area, the French IFREMER (Institut Français de Recherche pour l'Exploitation de la Mer) area and the Polish IOM (InterOceanMetal) area. In order to determine the disturbance depths of the different small-scale disturbances in the different European contract areas, we correlate the depth distributions of solid-phase Mn and total organic carbon (TOC) between disturbed sites and undisturbed reference sites using the Pearson product-moment correlation coefficient. On this basis, we (1) assess the short- and long-term consequences of small-scale disturbances on redox zonation and element fluxes and (2) determine how much time is needed for the re-establishment of a new steady state geochemical system in the sediments after the disturbances. Our work includes pore-water and solid-phase analyses as well as the application of a transient one-dimensional transport-reaction model.

2. Material and methods

As part of the European JPI Oceans pilot action "Ecological Aspects of Deep-Sea Mining (MiningImpact)", multiple corer (MUC) and gravity corer (GC) sediment cores were taken during RV SONNE cruise SO239 in March/April 2015 from undisturbed sites in various European contract areas for the exploration of polymetallic nodules (Fig. 1; Table 1; Martínez Arbizu and Haeckel, 2015). These undisturbed reference sites were chosen in close proximity (< 5 km) to small-scale disturbance experiments for the simulation of deep-sea mining, which were created up to 37 yr ago and re-visited during cruise SO239 (Table 1; see Sect. 2.1.1.; Martínez Arbizu and Haeckel, 2015). The sampling of sediments in the disturbance tracks of these experiments were conducted by video-guided push-coring (PC) between 1 day and 37 yr after the initial disturbances using the ROV Kiel 6000 (Table 1; Fig. 2; Martínez Arbizu and Haeckel, 2015).

The different investigated European contract areas within the CCZ include the BGR, IOM, GSR and IFREMER areas. Comprehensive pore-water and solid-phase analyses on the MUC and GC sediment cores from undisturbed sites have been conducted in previous baseline studies and are presented elsewhere (Volz et al., 2018; Volz et al., 2020). These analyses include the determination of pore-water oxygen, NO_3^-, Mn^{2+} and NH_4^+ concentrations and contents of total organic carbon (TOC) for MUC and GC sediment cores (Volz et al., 2018) as well as solid-phase bulk Mn contents for the MUC sediment cores (Volz et al., 2020). In the framework of this study, we have used these previously published pore-water and solid-phase data as undisturbed reference data for geochemical conditions and sediment composition (Table 1). On this basis, here, we investigate seven small-scale disturbances for the simulation of deep-sea mining (Table 1; see Sect. 2.1.1.; Martínez Arbizu and Haeckel, 2015).

2.1. Site Description

The CCZ is defined by two transform faults, the Clarion Fracture Zone in the north and the Clipperton Fracture Zone in the south and covers an area of about 6 million km^2 (Fig. 1; e.g., Halbach et al., 1988). The sediments at the investigated sites (Table 1) are dominated by clayey siliceous oozes with Mn nodules varying in size (1–10 cm) and spatial density (0–30 kg m^{-2}) at the sediment surface (Berger, 1974; Kuhn et al., 2012; Mewes et al., 2014; Volz et al., 2018). In order to characterize the investigated sediments with respect to redox zonation, sedimentation rates, fluxes of particulate organic carbon (POC) to the seafloor and bioturbation depths, we have summarized these key parameters, which are originally presented elsewhere, in Table 2 (Volz et al., 2018). Steady state transport-reaction models have shown that aerobic respiration is the dominant biogeochemical process at all investigated sites, consuming more than 90 % of the organic matter delivered to the seafloor (Mogollón et al., 2016; Volz et al., 2018). Below the OPD at more than 0.5 m depth, Mn(IV) and nitrate reduction succeeds in the suboxic zone, where oxygen and sulfide are absent (e.g., Mewes et al., 2014; Mogollón et al., 2016; Kuhn et al., 2017b; Volz et al., 2018). At several sites investigated in this study, including the BGR "reference area" (BGR-RA) and IOM sites, decreasing Mn^{2+} concentrations at depth are probably associated with the oxidation of Mn^{2+} by upward diffusing oxygen circulating through the underlying basaltic crust (Volz et al., 2018; Mewes et al., 2016; Kuhn et al., 2017b).

2.1.1. Small-scale disturbances

Since the 1970s, several comprehensive environmental impact studies of deep-sea mining simulations have been carried out in the CCZ, including the Benthic Impact Experiment (BIE; e.g., Trueblood and Ozturgut, 1997; Radziejewska, 2002) and the Japan Deep Sea Impact Experiment (JET; Fukushima, 1995). In addition, numerous small-scale seafloor disturbances have been carried out in the CCZ in the past 40 yr using various tools such as epibenthic sleds (EBS) and dredges (e.g., Vanreusel et al., 2016; Jones et al., 2017). The EBS is towed along the seabed for the collection of benthic organisms (and nodules) thereby also removing the upper few centimeters of the sediments (e.g., Brenke, 2005). In 2015, some of these up to 37 yr old disturbances were re-visited as part of the BMBF-EU JPI Oceans pilot action "Ecological Aspects of Deep-Sea Mining (MiningImpact)" project in order to evaluate the long-term consequences of such small-scale disturbances on the abyssal benthic ecosystem (Table 1; Fig. 2; Martínez Arbizu and Haeckel, 2015). For comparison, the Disturbance and

Recolonization Experiment (DISCOL), which was conducted in a nodule field in the Peru Basin (PB) in 1989 was re-visited as part of MiningImpact (Boetius, 2015; Greinert, 2015). In the framework of DISCOL, a seafloor area of ~ 11 km^2 was disturbed with a plough harrow. The impact of the DISCOL experiment was studied 0.5, 3 and 7 yr after the disturbance had been set (e.g., Thiel, 2001). Furthermore, new small-scale disturbance tracks were created during SO239 in the BGR-RA and in the GSR area "B6" using an EBS in order to add also initial temporal datasets (Table 1; Fig. 2; Martínez Arbizu and Haeckel, 2015). The EBS weighed about 400 kg and created a disturbance track of about 1.5 m width (Brenke, 2005). The fresh EBS disturbance tracks in the BGR-RA and GSR areas were re-visited 1 day after their creation. Eight months prior to the cruise SO239, towed dredge sampling was performed in the GSR area by the Belgian contractor (Martínez Arbizu and Haeckel, 2015; Jones et al., 2017). During the BIONOD cruises onboard RV L'Atalante in 2012, the same EBS setup as used during cruise SO239 was deployed in the BGR "prospective area" (BGR-PA) and in the IFREMER area (Table 1; Rühlemann and Menot, 2012; Menot and Rühlemann, 2013; Martínez Arbizu and Haeckel, 2015). In 1995, the Deep-Sea Sediment Re-suspension System (DSSRS) was used during the IOM-BIE (Benthic Impact Experiment) disturbance in the IOM area (Table 1; e.g., Kotlinski and Stoyanova, 1998). The DSSRS weighed 3.2 tons under normal atmospheric pressure and was designed to dredge the seafloor while producing a re-suspended particle plume about 5 m above the seafloor (Brockett and Richards, 1994; Sharma, 2001). Based on the dimensions of the DSSRS device, the disturbance track created during the IOM-BIE disturbance experiment is about 2.5 m wide (Fig. 2; Brockett and Richards, 1994). In 1978, the Ocean Mineral Company (OMCO) created disturbance tracks in the French IFREMER area by towed dredge sampling (Table 1; e.g., Spickermann, 2012).

2.2. Sediment sampling and solid-phase analyses

ROV-operated push cores were sampled at intervals of 1 cm for solid-phase analyses. Bulk sediment data and TOC contents have been corrected after Kuhn (2013) for the interference of the pore-water salt matrix with the sediment composition (Volz et al., 2018). The mass percentage of the pore water was determined gravimetrically before and after freeze drying of the wet sediment samples. The salt-corrected sediment composition c' was calculated from the measured solid-phase composition c using the mass percentage of H_2O of the wet sediment (w), which contains 96.5 % H_2O (Eq. (1)).

$$c' = c * \frac{100}{100 - \left(100 * \frac{\left(w * \frac{100}{96.5}\right) - w}{100 - w}\right)} \quad (1)$$

2.2.1. Total acid digestions

Total acid digestions were performed in the microwave system MARS Xpress (CEM) after the protocols by Kretschmer et al. (2010) and Nöthen and Kasten (2011). Approximately 50 mg of freeze-dried, homogenized bulk sediment were digested in an acid mixture of 65 % sub-boiling distilled HNO_3 (3 mL), 30 % sub-boiling distilled HCl (2 mL) and 40 % suprapur® HF (0.5 mL) at ~ 230 °C. Digested solutions were fumed off to dryness, the residue was re-dissolved under pressure in 1 M HNO_3 (5 mL) at ~ 200 °C and then filled up to 50 mL with 1 M HNO_3. Total bulk Mn and Al contents were determined using inductively coupled plasma optical emission spectrometry (ICP-OES; IRIS Intrepid ICP-OES Spectrometer, Thermo Elemental). Based on the standard reference material NIST 2702 accuracy and precision of the analysis was 3.7 % and 3.5 % for Mn, respectively (n=67).

2.2.2. Total organic carbon

Total organic carbon (TOC) contents were determined using an Eltra CS2000 element analyzer. Approximately 100 mg of freeze-dried, homogenized sediment were transferred into a ceramic cup and decalcified with 0.5 mL of 10 % HCl at 250 °C for 2 h before analysis. Based on an in-house reference material, precision of the analysis was better than 3.7 % (n=83).

2.3. Pearson correlation coefficient

In order to determine the disturbance depths, solid-phase bulk Mn contents were correlated between disturbed sediments and undisturbed reference sediments using the Pearson product-moment correlation coefficient r (Eq. (2); Table 1; Pearson, 1895). The Pearson correlation coefficient is a statistical measure of the linear relationship between two arrays of variables with:

$$r_{xy} = \frac{\sum_{i=1}^{n}(x_i - \bar{x})(y_i - \bar{y})}{\sqrt{\sum_{i=1}^{n}(x_i - \bar{x})^2 \sum_{i=1}^{n}(y_i - \bar{y})^2}} \tag{2}$$

where n is the sample size, x and y are individual sample points and $\bar{x}$ and $\bar{y}$ are the sample means $\bar{x} = \frac{1}{n}\sum_{i=1}^{n} x_i$ and $\bar{y} = \frac{1}{n}\sum_{i=1}^{n} y_i$.

While the solid-phase bulk Mn contents of the disturbed sediments were determined in the framework of this study, solid-phase bulk Mn contents from undisturbed reference sediments were taken from Volz et al. (2020). The highest positive linear correlations of solid-phase Mn contents (r_{Mn} ~ 1) between the disturbed sites and the respective undisturbed reference sites (Table 1) were used to determine the depths of the disturbances. In a second step, the same correlation was applied to the TOC contents (r_{TOC}) in order to verify the depth of disturbance. While the TOC contents in the disturbed sediments were determined in the framework of this study, TOC contents from undisturbed reference sediments were taken from Volz et al. (2018).

2.4. Geochemical model setup and reaction network

A transient one-dimensional transport-reaction model (Eq. (3); e.g., Boudreau, 1997; Haeckel et al., 2001) was used (1) to assess the impact of small-scale disturbances on biogeochemical processes, geochemical conditions and element fluxes in sediments of the CCZ and (2) to estimate the time required to establish a new steady state geochemical system after a small-scale disturbance. We have applied a transient transport-reaction model for the sites in the BGR-RA and IOM areas (Table 1). These sites were chosen due to distinctively different sedimentation rates and OPD (Table 2). We have adapted the code of the steady state transport-reaction model, which was originally presented by Volz et al. (2018) and used pore-water oxygen, NO_3^-, Mn^{2+} and NH_4^+ data as well as TOC contents of GC sediment cores from the same study as undisturbed reference data (Table 1; Table 2). Thus, the model parameters and baseline input data used for the transient transport-reaction model are the same as presented in the study by Volz et al. (2018). The transient transport-reaction model consists of four aqueous (O_2, NO_3^-, Mn^{2+}, NH_4^+), four solid species ($TOC_{1\text{-}3}$, MnO_2) and six reactions (R_1-R_6; Supplementary Table 1) with:

$$\frac{\partial(\vartheta_i C_{i,j})}{\partial t} = \frac{\partial D_{i,j}\vartheta_i\left(\partial C_{i,j}/\partial z\right)}{\partial z} - \frac{\partial \omega_i \vartheta_i C_{i,j}}{\partial z} + \alpha_i \vartheta_i \left(C_{i,j} - C_{0,j}\right) + \vartheta_i \sum R_{i,j} \qquad (3)$$

where z is sediment depth, and subscripts i, j represent depth and species-dependence, respectively; aqueous or solid species concentration are denoted by C (Supplementary Table 2); D is in case of solutes the effective diffusive mixing coefficient, which has been corrected for tortuosity ($D_{m,i,j}$; Boudreau, 1997). In the case of solids, D represents the bioturbation coefficient (B_i; Eq. (4)); ϑ is the volume fraction representing the porosity φ for the aqueous phase and $1 - \varphi$ for the solid phase; the velocity of either the aqueous (v) or the solid phase (w) is denoted by the symbol ω ; α_i is the bioirrigation coefficient (0 for solid species; Eq. (5)); and $\sum R_{i,j}$ is the sum of the reactions affecting the given species.

The bioturbation and bioirrigation profiles, i.e. biologically induced mixing of sediment and pore water, are represented by a modified logistic function:

$$B_i = B_0 \exp\left(\frac{z_{mix} - z_i}{z_{att}}\right) / \left(1 + \exp\left(\frac{z_{mix} - z_i}{z_{att}}\right)\right) \qquad (4)$$

$$\alpha_i = \alpha_0 \exp\left(\frac{z_{mix}-z_i}{z_{att}}\right) / \left(1 + \exp\left(\frac{z_{mix}-z_i}{z_{att}}\right)\right) \quad (5)$$

where α_0 and B_0 are constants indicating the maximum biorrigation and bioturbation intensity at the sediment-water interface; the depth where the bioturbation and bioirrigation intensity is halved is denoted by z_{mix} ; and the attenuation of the biogenically induced mixing with depth is controlled by z_{att}.

Assuming steady state compaction, the model applies an exponential function that is parameterized according to the available porosity data at each station (e.g., Berner, 1980; Supplementary Fig. 1):

$$\varphi_i = \varphi_\infty (\varphi_0 - \varphi_\infty) \exp(-\beta z) \quad (6)$$

where φ_∞ is the porosity at the 'infinite depth', at which point compaction is completed; φ_0 is the porosity at the sediment water interface ($z = 0$) ; and β is the porosity-attenuation coefficient.

Organic matter was treated in three reactive fractions (3G-model) with first order kinetics. The rate expressions for the reactions (R_1-R_6) include inhibition terms, which are listed together with the rate constants (Supplementary Table 3).

Based on the Pearson correlation coefficient r_{Mn}, we have removed the upper 7 cm of sediments in the transport-reaction model for the IOM-BIE site and the upper 10 cm of sediments in the transport-reaction model for the BGR-RA site. Due to the lack of data on the re-establishment of bioturbation, i.e. the recovery of the bioturbation 'pump' after small-scale disturbance experiments, we have tested the effect of different bioturbation scenarios in the transport-reaction model. For the different post-disturbance bioturbation scenarios, we have assumed that bioturbation is inhibited immediately after the disturbance with a linear increase to undisturbed reference bioturbation coefficients (Volz et al., 2018). Based on the work by Miljutin et al. (2011) and Vanreusel et al. (2016), we have assumed that bioturbation should be fully re-established after 100, 200, and 500 yr. As the modelling results for the different time spans were almost identical, we only present here the model that assumes bioturbation is at pre-disturbance intensity 100 yr after the impact (Volz et al., 2018; Supplementary Table 2). We have applied the transient transport-reaction model under the assumption that the sedimentation rates as well as the POC fluxes to the seafloor remain constant over time (Table 2). The model was coded in MATLAB with a discretization and reaction set-up closely following the steady state model (Volz et al., 2018).

3. Results

3.1. Characterization of disturbed sites

Most of the small-scale disturbances investigated in the framework of this study were created with an EBS (Table 1; Fig. 2). Based on the visual impact inspection of the EBS disturbance tracks in the CCZ, the sediments were mostly pushed aside by the EBS and piled up next to the left and right of the tracks (Fig. 2). In particular, the freshly created 1-day old EBS tracks in the BGR-RA and GSR areas indicate that the sediments were mostly scraped off and accumulated next to the freshly exposed sediment surfaces (Fig. 2). Small sediment lumps occur on top of the exposed sediment surfaces on the EBS tracks, which indicates that some sediment has slid off from the adjacent flanks of the sediment accumulation after the disturbances (Fig. 2). However, the mostly smooth sediment surfaces of the EBS tracks suggest that sediment mixing during the EBS disturbance experiments may be mostly negligible (Fig. 2; Table 1). In the 8-months old dredge track in the GSR area, small furrows occur at the disturbed sediment surface most likely caused by the shape of the dredge (Fig. 2).

3.2. Sediment porosity and solid-phase composition

The sediment porosity shows little lateral variability and ranges between 0.65 and 0.8 throughout the upper 25 cm of the sediments at all investigated disturbed sites (Fig. 3). At the disturbed IOM-BIE site, sediment porosity is about 5 % higher in the upper 4 cm of the sediments than below. Bulk Mn contents in the upper 25 cm of the sediments at the disturbed sites are between 0.1 and 0.9 wt% (Fig. 3). Solid-phase Mn contents decrease with depth at all investigated sites. Total organic carbon (TOC) contents in the upper 25 cm of the sediments at the disturbed sites are within 0.2 and 0.5 wt% (Fig. 3). The TOC contents slightly decrease with depth at all investigated sites.

3.3. Pearson correlation coefficient and disturbance depths

The Pearson correlation coefficient r_{Mn} for the correlation of solid-phase Mn contents between the disturbed sites and the respective reference sites ranges between 0.72 and 0.97 (Table 3). Based on r_{Mn}, 5-15 cm of sediment has been removed by various disturbance experiments in the different contract areas (Fig. 4). Applying these r_{Mn}-derived disturbance depths for the correlation of the TOC depth distributions between disturbed sites and respective adjacent reference sites gives Pearson correlation coefficients r_{TOC} within 0.73 and 0.91 (Table 3; Fig. 4), which may support the estimates for the disturbance depth based on r_{Mn}. At the BGR-RA site, the correlation of TOC contents between the disturbed site and the reference site shows negative values. As the sediment porosity in the disturbed sediments correlates well with the porosity in the respective undisturbed reference sediments (Fig. 4), sediment compaction due to the weight of the disturbance device may be negligible during the small-scale disturbances investigated in the framework of this study.

3.4. Transport-reaction modelling

The removal of the surface sediments in the transient transport-reaction model for the BGR-RA and IOM-BIE sites is associated with the loss of the reactive labile organic matter (Fig. 5 and 6). About 10 kyr after the removal of the upper 10 cm of the sediments in the model for the BGR-RA site, oxygen penetrates about tenfold deeper into the disturbed sediments than in undisturbed sediments (Table 2; Fig. 5; Volz et al., 2018). At the IOM-BIE site, oxygen reaches the maximum OPD at about 100 yr after the removal of the upper 7 cm of the sediments. At this site, the oxygen front migrates only ~ 1 m deeper than the corresponding OPD in undisturbed sediments (Table 2; Fig. 5; Volz et al., 2018). As a consequence of deeper OPDs at both sites, the oxic-suboxic redox boundary is located at greater depth, with a significant consumption of pore-water Mn^{2+} in the path of the oxygen front. The NH_4^+ concentrations are also being diminished, reaching minima within 100-1000 yr and 1-10 yr after the disturbance experiments in the BGR-RA and IOM areas, respectively. The trend for the NO_3^- is more complicated with lower concentrations during the downward migration of the OPD and augmented concentrations once oxygen concentrations reach their maximum (Figs. 5 and 6).

Naturally, the solute fluxes across the sediment-water interface (SWI) are strongly affected after the surface sediment removal (Fig. 7). The transient transport-reaction model suggests that the oxygen fluxes into the sediments are lowered by a factor of three to six after 10-100 yr at the IOM-BIE and BGR-RA sites, respectively. This trend is mirrored by the decreased release of NH_4^+ and NO_3^- into the bottom water.

4. Discussion

4.1. Depths of small-scale disturbance experiments

Our work demonstrates that the depth distribution of solid-phase Mn provides a reliable tool for the determination of the disturbance depths in the sediments of the CCZ (Fig. 4; Table 3). The success of the correlation of solid-phase Mn contents between disturbed and undisturbed reference sediments benefits from several factors:

(1) Sediment mixing during the small-scale disturbance experiments is negligible: The visual impact assessment of the investigated disturbance tracks in the CCZ suggests that sediment mixing during the small-scale disturbance experiments was insignificant (Fig. 2). This

observation is in agreement with a recent EBS disturbance experiment, which has been conducted in the DISCOL area in 2015 (Greinert, 2015). The freshly created EBS track in the DISCOL area was re-visited 5 weeks after the disturbance experiment, where the surface sediment was mostly removed and deeper sediment layers were exposed without visible sediment mixing (Boetius, 2015; Paul et al., 2018). In a study on the geochemical regeneration in disturbed sediments of the DISCOL area in the Peru Basin, Paul et al. (2018) have shown that the bulk Mn-rich top sediment layer, which has been observed in undisturbed sediments, is removed in the 5-week old EBS disturbance track. Thus, an important pre-requisite for this method is met and the authors have proposed that the depth distribution of solid-phase Mn may be suitable for the evaluation of the impact as well as for the monitoring of the recovery of small-scale disturbance experiments.

(2) The fact that the solid-phase Mn maxima in the surface sediments appear to be a regional phenomenon across the CCZ area as it has been observed throughout the different exploration areas studied in the framework of this study (Volz et al., 2020): The investigated disturbed sediments as well as the undisturbed reference sediments in the CCZ show decreasing solid-phase Mn contents with depth in the upper 20-30 cm of the sediments (Fig. 3; Fig. 4; Volz et al., 2020). In the undisturbed reference sediments, solid-phase Mn contents show maxima of up to 1 wt% in the upper 10 cm of the sediments with distinctly decreasing contents below (Fig. 4; Volz et al., 2020). Similar bulk solid-phase Mn distribution patterns have been reported for other sites within the CCZ (e.g., Khripounoff et al., 2006; Mewes et al., 2014; Widmann et al., 2014). Volz et al. (2020) have suggested that the widely observed solid-phase Mn enrichments in CCZ surface sediments formed in association with a more compressed oxic zone, which may have prevailed as a result of lower bottom-water oxygen concentrations during the last glacial period than today. Strong indication for lower glacial bottom-water oxygen concentrations throughout the eastern Pacific Ocean have been provided by a number of independent proxies (e.g., Anderson et al., 2019 and references therein). As a consequence of the condensed oxic zone, upward diffusing pore-water Mn^{2+} may have precipitated as authigenic Mn(IV) at a shallow oxic-suboxic redox boundary in the upper few centimeters of the sediments. After the last glacial period, the authigenic Mn(IV) peak was continuously mixed into subsequently deposited sediments by bioturbation causing the observed broad solid-phase Mn(IV) enrichment in the surface sediments (Fig. 4; Volz et al., 2020).

(3) Lastly, the OPD at all sites is located at sediment depths greater than 0.5 m, and thus, diagenetic precipitation of Mn(IV) in the surface sediments (e.g. Gingele and Kasten, 1994) since the last glacial period can be ruled out (Table 2; Mewes et al., 2014; Volz et al., 2020).

Based on the depth distribution of solid-phase Mn, our work suggests that between 5 and 15 cm of the surface sediments were removed and pushed aside by the different small-scale disturbance experiments in the CCZ (Table 3; Fig. 4). This range of disturbance depths is in good agreement with other estimates for small-scale disturbances by similar gear in the CCZ and in the DISCOL area, which suggest that the upper 4-20 cm of the sediments were removed (e.g., Thiel, 2001; Oebius et al., 2001; König et al., 2001; Grupe et al., 2001; Radziejewska, 2002; Khripounoff et al., 2006; Paul et al., 2018). However, as the disturbed sites investigated in this study and the respective undisturbed reference sites are located up to 5 km apart from each other, the correlation of solid-phase Mn may be influenced by some spatial heterogeneities in solid-phase Mn contents (Table 1; Mewes et al., 2014). Furthermore, it should be noted, that for the correlation of solid-phase Mn contents between the disturbed and undisturbed reference sites, we have not considered that (1) particles may have re-settled on the freshly exposed sediment surfaces from re-suspended particle plumes (e.g., Jankowski and Zielke, 2001; Thiel, 2001; Radziejewska, 2002; Gillard et al., 2019), (2) sediment has slid off from adjacent flanks of the sediment accumulation after the disturbances (Fig. 2) and (3) sediments have been deposited after the small-scale disturbances at sedimentation rates between 0.2 and 1.2 cm kyr^{-1} (Table 2; Volz et al., 2018). However, only in the case of the IOM-BIE disturbance, the visual impact assessment suggested that the disturbance surface was concealed, here by re-settling sediments (Fig. 2). The development of a re-suspended particle plume during the disturbance experiments highly depends on various factors, such as sediment properties, seafloor topography, bottom-water currents and the disturbance device (e.g., Gillard et al., 2019). Although local and regional variations in these factors have been reported for the CCZ, they are not well constrained (e.g., Mewes et al., 2014; Aleynik et al., 2017; Volz et al., 2018; Gillard et al., 2019; Hauquier et al., 2019). As the disturbance tracks investigated in the framework of this study are relatively small with a maximum width of 2.5 m (Fig. 2; Brockett and Richards, 1994; Brenke 2005), re-suspended particles may (1) only partly deposit on the disturbance track and (2) mostly be transported laterally by currents and deposit on top of undisturbed sediments in the proximity of the disturbance tracks (e.g., Fukushima, 1995; Aleynik et al., 2017; Gillard et al., 2019). This is in accordance with the close correlation of the sediment porosity between the disturbed and undisturbed reference sites, which indicates that the deposition of re-settling particles with higher porosity at the sediment surface in the disturbance tracks is insignificant at all sites, except for the IOM-BIE site (Fig. 4). The porosity data further shows that sediment compaction, potentially caused by the weight of the disturbance device (Cuvelier et al., 2018; Hauquier et al., 2019) is insignificant at all disturbed sites.

4.2. Impact of small-scale disturbances on the geochemical system

The geochemical conditions found at the study sites in the CCZ are the result of a balanced interplay of key factors, such as the input of fresh, labile TOC, sedimentation rate and bioturbation intensity (e.g., Froelich et al., 1979; Berner, 1981; Zonneveld et al., 2010; Mogollón et al., 2016; Volz et al., 2018). Together they characterize the upper reactive layer, which in turn plays a crucial role for the location of the OPD in the sediments of the CCZ (e.g., Mewes et al., 2014; Mogollón et al., 2016; Volz et al., 2018). Oxygen is consumed via aerobic respiration during the degradation of organic matter while bioturbation transports fresh, labile TOC into deeper sediments (e.g., Haeckel et al., 2001; König et al., 2001). The presence of labile TOC throughout the bioturbated zone significantly enhances the consumption of oxygen with depth, where oxygen is not as easily replenished by seawater oxygen. Thus, the availability of labile TOC in the bioturbated layer controls the amount of oxygen that passes through the reactive layer into deeper sediments (e.g., König et al., 2001). Below the highly reactive layer, refractory organic matter degradation and secondary redox reactions – such as oxidation of Mn^{2+} – control the consumption of oxygen (Supplementary Table 1; Mogollón et al., 2016; Volz et al., 2018). The oxygen profile, more precisely the position of the OPD, in turn, strongly influences the distribution of other solutes. Below the OPD, denitrification and Mn(IV) reduction commence, albeit at much lower rates, consuming pore-water NO_3^- and releasing Mn^{2+} (Mogollón et al., 2016; Volz et al., 2018). The study sites in the CCZ provide an excellent example for how slight differences in key environmental factors can profoundly change the overall solute profiles with OPDs ranging between 0.5 m (BGR-RA) and > 7.4 m (GSR) as outlined by Volz et al. (2018).

The removal of the upper 5-15 cm of the sediment results, on one hand, in an almost complete loss of the labile TOC fraction (Fig. 4) as this fraction is restricted to the upper 20 cm of the sediment in the CCZ (e.g., Müller and Mangini, 1980; Emerson, 1985; Müller et al., 1988; Mewes et al., 2014; Mogollón et al., 2016; Volz et al., 2018). On the other hand, studies on faunal diversity and density in small-scale disturbances in the sediments of the CCZ and in the DISCOL area show that most of the biota is lost immediately after the disturbance experiment (Borowski et al., 1998; 2001; Bluhm et al., 2001; Thiel et al., 2001; Vanreusel et al., 2016;

Jones et al., 2017; Gollner et al., 2017). Thus, a drastic decline or stand-still of bioturbation can be expected in the surface sediments.

Based on the results of the transient transport-reaction model, geochemical recovery after small-scale sediment disturbances can be divided into two main phases (Fig. 8):

(1) Since the labile TOC fraction and bioturbating fauna is mostly removed, downward diffusion of oxygen is the main driver shaping solute profiles towards a new geochemical steady state system in the absence of the reactive layer (Figs. 5 and 6). This entails the downward migration of the OPD, as oxygen is no longer effectively consumed in the upper sediment layer. The presence of oxygen outcompetes denitrification and Mn(IV) reduction and induces NH_4^+ and Mn^{2+} oxidation instead, thus, minimizing pore-water NH_4^+ and Mn^{2+} concentrations (Figs. 5 and 6). At the same time, NO_3^-, produced during nitrification in the presence of oxygen (e.g., Froelich et al., 1979; Berner, 1981; Haeckel et al., 2001; Mogollón et al., 2016; Volz et al., 2018), is accordingly reduced during denitrification and NO_3^- concentrations are lowered during this first phase.

(2) The second phase is characterized by the increasing influence of reactive fluxes across the seafloor. It takes approximately 1000 yr before any significant build-up of an upper labile TOC layer is re-established (Fig. 6), at which point solute profiles slowly shift towards their pre-disturbance shape (Fig. 7). Interestingly, during the transition time when oxygen is still present at depth but aerobic respiration in the upper sediments has already began to pick up, NO_3^- concentrations are strongly elevated in the BGR sediments (Figs. 5 and 6). This is due to the fact that NO_3^- is not consumed during denitrification or the Mn-annamox reaction in the presence of oxygen (Mogollón et al., 2016; Volz et al., 2018).

With the importance of bioturbation and the mining-related removal of associated fauna in mind, solute and in particular nutrient fluxes across the seafloor should also be considered. The release of nutrients complements the close link between sediment geochemistry and the food web structure (e.g., Smith et al., 1979; Dunlop et al., 2016; Stratmann et al., 2018) and further emphasizes their interdependencies. Figure 7 depicts fluxes of oxygen, NO_3^- and NH_4^+ across the seafloor. As expected, with the reactive layer being mostly absent, fluxes across the seafloor are severely reduced, which particularly affects the oxygen uptake of the sediments as well as the release of NO_3^- and NH_4^+ into the bottom water. At about 100 to 1000 yr after the disturbance, concurrent with the build-up of an upper sediment layer containing significant amounts of labile organic matter, fluxes begin to increase again, albeit much slower than the rate of the decrease in fluxes subsequently after the disturbances (Fig. 7, note the logarithmic scale).

It should be noted that while bioturbation has a pivotal influence on the undisturbed steady-state profile, it only plays a secondary role in re-establishing the steady state geochemical system at the disturbed sites in the CCZ. Studies suggest that faunal abundances fully recover within centuries after the disturbance even though the benthic community may be different than prior to the disturbance (e.g., Miljutin et al., 2011; Vanreusel et al., 2016). Due to the extremely slow build-up of the reactive layer with labile TOC, the bioturbation 'pump' is active again before any significant amount of labile TOC is present about 1-100 kyr after the disturbance. Thus, full recovery is mainly controlled by the re-establishment of the upper reactive layer, i.e. the delivery rate of labile TOC to the seafloor.

The transport-reaction model reveals that under current depositional conditions, the new steady state geochemical system is established after 1-10 kyr at the IOM-BIE site, while the re-establishment of steady state geochemical conditions at the BGR-RA site takes 10-100 kyr (Figs. 5 and 6). Shorter recovery times at the IOM site compared to the BGR-RA site are related to higher sedimentation rates (1.15 instead of 0.65 cm kyr^{-1}) and shallower impact on the sediment (7 cm instead of 10 cm sediment removal). Accordingly, the maximum OPD is reached after 100 yr and 10 kyr at the IOM and BGR-RA site, respectively (Figs. 5 and 6) while the reactive layer is clearly established sooner at the IOM site compared to the BGR-RA site (Fig. 7). Thus, the disturbance depth clearly has a strong influence on the recovery process of the geochemical system of the sediments, highlighting the importance of low-impact mining equipment. Considering that in the CCZ areas of about 8500 km^2 could be commercially mined in 20 yr per individual mining operation (Madureira et al., 2016), this impact assessment of small-scale disturbance experiments may only represent a first approach for the prediction of the environmental impact of large-scale deep-sea mining activities.

5. Conclusion

We have studied surface sediments from seven small-scale disturbance experiments for the simulation of deep-sea mining, which were performed between 1 day and 37 years prior to our sampling in the NE Pacific Ocean. These small-scale disturbance tracks were created using various disturbance devices in different European contract areas for the exploration of polymetallic nodules within the eastern part of the Clarion-Clipperton Zone (CCZ). Through correlation of solid-phase Mn contents of disturbed and undisturbed reference sediments, we (1) propose that the depth distribution of solid-phase Mn in the sediments of the CCZ provides a reliable tool for the estimation of the disturbance depth and (2) show that 5-15 cm of the sediments were removed during the small-scale disturbance experiments investigated in this study. As the small-scale disturbances are associated with the removal of the surface sediments characterized by reactive labile organic matter, the disturbance depth ultimately determines the impact on the geochemical system in the sediments. The application of a transient transport-reaction model reveals that the removal of the upper 7-10 cm of the surface sediments is associated with a meter-scale downward extension of the oxic zone and the shutdown of denitrification and Mn(IV) reduction. As a consequence of lower respiration rates after the disturbance experiments, the geochemical system in the sediments is controlled by downward oxygen diffusion. While the re-establishment of bioturbation within centuries after the disturbance is important for the development of steady state geochemical conditions in the disturbed sediments, the rate at which geochemical steady state conditions are reached ultimately depends on the delivery rate of organic matter to the seafloor. Assuming the accumulation of labile organic matter to proceed at current Holocene sedimentation rates in the disturbed sediments, biogeochemical reactions resume in the reactive surface sediment layer, and thus, the new steady state geochemical system in the disturbed sediments in the CCZ is reached on a millennial time scale after the disturbance of the surface sediments.

Our study represents the first study on the impact of small-scale disturbance experiments on the sedimentary geochemical system in the prospective areas for polymetallic nodule mining in the CCZ. Our findings on the evaluation of the disturbance depths using solid-phase Mn contents as well as the quantification of the development of a new geochemical steady state system in the sediments advances our knowledge about the potential long-term consequences of deep-sea mining activities. We propose that mining techniques potentially used for the potential commercial exploitation of nodules in the CCZ may remove less than 10 cm of the surface sediments in order to minimize the impact on the geochemical system in the sediments. The depth distribution of solid-phase Mn may be used for environmental monitoring purposes during future mining activities in the CCZ. However, based on our current knowledge and in combination with ongoing natural environmental changes (e.g., bottom water warming, acidification, changes in the POC flux to the seafloor), it is difficult to assess whether the surface sediment removal may trigger a tipping point for deep-sea ecosystems. This study also provides valuable data for further investigations on the environmental impact of deep-sea mining, such as during the launched JPI Oceans follow-up project MiningImpact 2.

Data availability

The data are available via the data management portal OSIS-Kiel and the WDC database PANGAEA, including the solid-phase bulk sediment Mn and TOC contents (https://doi.org/10.1594/PANGAEA.904560) as well as the porosity data (https://doi.org/10.1594/PANGAEA.904578).

Author contribution

The study was conceived by all co-authors. JBV carried out the sampling and analyses on board during RV SONNE cruise SO239 and the analytical work in the laboratories at AWI in Bremerhaven. LH and MH modified the numerical transport-reaction model presented in Volz et al. (2018) and provided model results for the long-term effects of small-scale disturbances on geochemical conditions and biogeochemical processes. JBV prepared the manuscript with substantial contributions from all co-authors.

Competing interest

The authors declare that they have no conflict of interest.

Acknowledgements

We thank captain Lutz Mallon, the crew and the scientific party of RV SONNE cruise SO239 for the technical and scientific support. Thanks to Jennifer Ciomber, Benjamin Löffler and Vincent Ozegowski for their participation in sampling and analysis onboard. For analytical support in the home laboratory and during data evaluation we are grateful to Ingrid Stimac, Olaf Kreft, Dennis Köhler, Ingrid Dohrmann (all at AWI). Special thanks to Prof. Dr. Gerhard Bohrmann (MARUM, University of Bremen), Dr. Timothy G. Ferdelman (MPI Bremen) and Dr. Ellen Pape (University of Ghent) for much appreciated discussions.

This study is funded by the Bundesministerium für Bildung und Forschung (BMBF Grant 03F0707A+G) as part of the JPI-Oceans pilot action “Ecological Aspects of Deep-Sea Mining (MiningImpact)”. We acknowledge further financial support from the Helmholtz Association (Alfred Wegener Institute Helmholtz Centre for Polar and Marine Research).

References

Aleynik, D., Inall, M. E., Dale, A., and Vink, A.: Impact of remotely generated eddies on plume dispersion at abyssal mining sites in the Pacific, Sci. Rep., 7, 1–14, doi:10.1038/s41598-017-16912-2, 2017.

Anderson, R.F., Sachs, J.P., Fleisher, M.Q., Allen, K.A., Yu, J., Koutavas, A., and Jaccard, S.L. Deep-sea oxygen depletion and ocean carbon sequestration during the last ice age. Global Biogeochem. Cycles, 33, 301-317, doi:10.1029/2018GB006049, 2019.

Berger, W. H.: Deep-sea sedimentation, in: The Geology of Continental Margins, edited by: Burk, C. A., and Drake, C. L., Springer, New York, 213–241, 1974.

Berner, R. A.: A new geochemical classification of sedimentary environments, J. Sediment. Petrol., 51, 359-365, 1981.

Berner, R. A.: Early Diagenesis: A Theoretical Approach, Princeton University Press, Princeton, 1-24, 1980.

Bluhm H.: Re-establishment of an abyssal megabenthic community after experimental physical disturbance of the seafloor, Deep-Sea Res. Part II Top. Stud. Oceanogr., 48, 3841–3868, 2001.

Boetius, A., and Haeckel, M.: Mind the seafloor, Science, 359, 34-36, doi:10.1126/science.aap7301, 2018.

Boetius, A.: RV Sonne Fahrtbericht / Cruise Report SO242-2: JPI OCEANS Ecological Aspects of Deep-Sea Mining, DISCOL Revisited, Guayaquil-Guayaquil (Equador), 28.08.-01.10.2015, Kiel: Helmholtz-Zentrum für Ozeanforschung, 2015.

Borowski, C.: Physically disturbed deep-sea macrofaunal impacts of a large-scale physical disturbance experiment in the Southeast Pacific, Deep-Sea Res. Part II Top. Stud. Oceanogr., 48, 3809–3839, 2001.

Borowski, C., and Thiel, H.: Deep-Sea macrofaunal impacts of a large-scale physical disturbance experiment in the Southeast Pacific, Deep-Sea Res. Part II Top. Stud. Oceanogr., 45, 55-81, 1998.

Boudreau, B. P.: A one-dimensional model for bed-boundary layer particle exchange, J. Mar. Syst., 11, 279–303, doi:10.1016/S0924-7963(96)00127-3, 1997.

Brenke, N.: An Epibenthic sledge for operations on marine soft bottom and bedrock, J. Mar. Tech. Soc., 39, 10–19, 2005.

Brockett, T., and Richards, C. Z.: Deep-sea mining simulator for environmental impact studies, Sea Technol., 35, 77-82, 1994.

Chung, J. S.: Full-Scale, Coupled Ship and Pipe Motions Measured in North Pacific Ocean: The Hughes Glomar Explorer with a 5,000-m-Long Heavy-Lift Pipe Deployed, Proc. 19th ISOPE, 20, 1-6, 2010.

Cronan, D. S., Rothwell, G., and Croudace, I.: An ITRAX geochemical study of ferromanganiferous sediments fromthe Penrhyn basin, South Pacific Ocean, Mar. Georesour. Geotechnol., 28, 207–221, doi:10.1080/1064119X.2010.483001, 2010.

Cuvelier, D., Gollner, S., Jones, D. O. B., Kaiser, S., Arbizu, P. M., Menzel, L., Mestre, N. C., Morato, T., Pham, C., Pradillon, F., Purser, A., Raschka, U., Sarrazin, J., Simon-Lledó, E., Stewart, I.M., Stuckas, H., Sweetman, A. K., and Colaço, A.: Potential Mitigation and Restoration Actions in Ecosystems Impacted by Seabed Mining, Front. Mar. Sci., 5, doi:10.3389/fmars.2018.00467, 2018.

Davies, A. J., Roberts, J. M., and Hall-Spencer, J.: Preserving deep-sea natural heritage: emerging issues in offshore conservation and management, Biol. Conserv., 138, 299–312, doi:10.1016/j.biocon.2007.05.011, 2007.

Dunlop, K. M., van Oevelen, D., Ruhl, H. A., Huffard, C. L., Kuhnz, L. A., and Smith, K. L.: Carbon cycling in the deep eastern North Pacific benthic food web: Investigating the effect of organic carbon input, Limnol. Oceanogr., 61, 1956–1968, https://doi.org/10.1002/lno.10345, 2016.

Emerson, S., Fischer, K., Reimers, C. and Heggie, D.: Organic carbon dynamics and preservation in deep-sea sediments, Deep-Sea Res., 32, 1–21, 1985.

Froelich, P. N., Klinkhammer, G. P., Bender, M. L., Luedke, L. A., Heath, G. R., Cullen, C., Dauphin, P., Hammond, D., Hartmann, B., and Maynard, V.: Early oxidation of organic matter in pelagic sediments of the Eastern Equatorial Pacific, suboxic diagenesis, Geochim. Cosmochim. Acta, 43, 1075-1090, 1979.

Fukushima, T.: Overview "Japan Deep-Sea Impact Experiment = JET", ISOPE-M-95-008, ISOPE, 1995.

Gillard, B., Purkiani, K., Chatzievangelou, D., Vink, A., Iversen, M. H., and Thomsen, L.: Physical and hydrodynamic properties of deep sea mining-generated, abyssal sediment plumes in the Clarion Clipperton Fracture Zone (eastern-central Pacific), Elem. Sci. Anth., 7, 2019.

Gingele, F. X., and Kasten, S.: Solid-phase manganese in Southeast Atlantic sediments: implications for the paleoenvironment. Mar. Geol., 121. 317-332, 1994.

Glasby, G. P.: Lessons Learned from Deep-Sea Mining. Science, 289, 551-553, doi:10.1126/science.289.5479.551, 2000.

Glover, A. G. and Smith, C. R.: The deep-sea floor ecosystem: current status and prospects of anthropogenic change by the year 2025, Environ. Conserv., 30, 219-241, 2003.

Gollner, S., Kaiser, S., Menzel, L., Jones, D. O. B., Brown, A., Mestre, N. C., van Oevelen, D., Menot, L., Colaço, A., Canals, M., Cuvelier, D., Durden, J. M., Gebruk, A., Egho, G. A., Haeckel, M., Marcon, Y., Mevenkamp, L., Morato, T., Pham, C. K., Purser, A., Sanchez-Vidal, A., Vanreusel, A., Vink, A., and Arbizu, P. M.: Resilience of benthic deep-sea fauna to mining activities, Mar. Environ. Res., 129, 76–101, doi:10.1016/j.marenvres.2017.04.010. 2017.

Greinert, J.: RV Sonne Fahrtbericht / Cruise Report SO242-1: JPI OCEANS Ecological Aspects of Deep-Sea Mining, DISCOL Revisited, Guayaquil-Guayaquil (Equador), 28.07.-25.08.2015, Kiel: Helmholtz-Zentrum für Ozeanforschung, 2015.

Grupe, B., Becker, H. J., and Oebius, H. U.: Geotechnical and sedimentological investigations of deep-sea sediments from a manganese nodule field of the Peru Basin, Deep. Res. Part II Top. Stud. Oceanogr., 48, 3593–3608, 2001.

Haeckel, M., König, I., Riech, V., Weber, M. E., and Suess, E.: Pore water profiles and numerical modelling of biogeochemical processes in Peru Basin deep-sea sediments, Deep. Res. Part II Top. Stud. Oceanogr., 48, 3713–3736, doi:10.1016/S0967-0645(01)00064-9, 2001.

Hauquier, F., Macheriotou, L., Bezerra, T. N., Egho, G., Martínez Arbizu, P., and Vanreusel, A.: Geographic distribution of free-living marine nematodes in the Clarion-Clipperton Zone: implications for future deep-sea mining scenarios, Biogeosciences, 16(18), 3475-3489. https://doi.org/10.5194/bg-16-3475-2019, 2019.

Halfar, J., and Fujita, R. M.: Precautionary management of deep-sea mining, Mar. Pol., 26, 103-106, 2002.

Halkyard, J. E.: Technology for Mining Cobalt Rich Manganese Crusts from Seamounts, Proc. OCEANS ’85, 352-274, 1985.

Halbach, P., Friedrich, G., and von Stackelberg, U. (Eds.): The manganese nodule belt of the Pacific Ocean, Enke, Stuttgart, 1988.

Hein, J. R., Mizell, K., Koschinsky, A., and Conrad, T. A.: Deep-ocean mineral deposits as a source of critical metals for high- and green-technology applications: comparison with land-based resources, Ore Geol. Rev., 51, 1–14, 2013.

Hoagland, P., Beaulieu, S., Tivey, M. A., Eggert, R. G., German, C., Glowka, L., and Lin, J.: Deep-sea mining of seafloor massive sulfides, Mar. Pol., 34, 728-732, doi:10.1016/j.marpol.2009.12.001, 2010.

International Seabed Authority (ISA): A Geological Model for Polymetallic Nodule Deposits in the Clarion-Clipperton Fracture Zone, Technical Study 6, Kingston, p. 211, 2010.

Jankowski, J. A., and Zielke, W.: The mesoscale sediment transport due to technical activities in the deep sea, Deep. Res. Part II Top. Stud. Oceanogr., 48, 3487–3521, 2001.

Jones, D. O. B., Kaiser, S., Sweetman, A. K., Smith, C. R., Menot, L., Vink, A., Trueblood, D., Greinert, J., Billett, D. S. M., Martínez Arbizu, P., Radziejewska, T., Singh, R., Ingole, B., Stratmann, T., Simon-Lledó, E., Durden, J. M., and Clark, M. R.: Biological responses to disturbance from simulated deep-sea polymetallic nodule mining, PLoS One, 12, e0171750, https://doi.org/10.1371/journal.pone.0171750, 2017.

Juan, C., Van Rooij, D., and De Bruycker, W.: An assessment of bottom current controlled sedimentation in Pacific Ocean abyssal environments, Mar. Geol., 403, 20–33, 2018.

Khripounoff, A., Caprais, J.-C., Crassous, P. and Etoubleau, J.: Geochemical and biological recovery of the disturbed seafloor in polymetallic nodule fields of the Clipperton-Clarion Fracture Zone (CCFZ) at 5,000-m depth, Limnol. Oceanogr., 51, 2033–2041, doi:10.4319/lo.2006.51.5.2033, 2006.

König, I., Haeckel, M., Lougear, A., Suess, E., and Trautwein, A. X.: A geochemical model of the Peru Basin deep-sea floor - and the response of the system to technical impacts, Deep. Res. Part II Top. Stud. Oceanogr., 48, 3737–3756, doi:10.1016/S0967-0645(01)00065-0, 2001.

Kotlinski R, and Stoyanova V.: Physical, Chemical, and Geological changes of Marine Environment Caused by the Benthic Impact Experiment at the IOM BIE Site, Proc. 8th ISOPE 2, 277-281, Montreal, Canada, 1998.

Kretschmer, S., Geibert, W., Rutgers van der Loeff, M. M., and Mollenhauer, G.: Grain size effects on 230Thxs inventories in opal-rich and carbonate-rich marine sediments, Earth Planet. Sci. Lett., 294, 131–142, doi:10.1016/j.epsl.2010.03.021, 2010.

Kuhn, G.: Don't forget the salty soup: Calculations for bulk marine geochemistry and radionuclide geochronology, Goldschmidt 2013 Florence, Italy, 25 August 2013 - 30 August 2013, doi:10.1180/minmag.2013.077.5.11, 2013.

Kuhn, T., Wegorzewski, A. V., Rühlemann, C., and Vink, A.: Composition, formation, and occurrence of polymetallic nodules, in: Deep-Sea Mining, edited by: Sharma, R., 23–63, Springer International Publishing, Cham., doi:10.1007/978-3-319-52557-0_2, 2017a.

Kuhn, T., Versteegh, G. J. M, Villinger, H., Dohrmann, I., Heller, C., Koschinsky, A., Kaul, N., Ritter, S., Wegorzewski, A. V. and Kasten, S.: Widespread seawater circulation in 18–22 Ma oceanic crust: Impact on heat flow and sediment geochemistry, Geology, 45, 799-802, doi:10.1130/G39091.1, 2017b.

Kuhn, T., Rühlemann, C., and Wiedicke-Hombach, M.: Developing a strategy for the exploration of vast seafloor areas for prospective manganese nodule fields, in: Marine Minerals: Finding the Right Balance of Sustainable Development and Environmental Protection, edited by Zhou, H., and Morgan, C. L., The Underwater Mining Institute, Gelendzhik, Russia (K 1-12), 2012.

Lodge, M., Johnson, D., Le Gurun, G., Wengler, M., Weaver, P., and Gunn, V.: Seabed mining: International Seabed Authority environmental management plan for the Clarion–Clipperton Zone. A partnership approach, Mar. Pol., 49, 66–72, doi:10.1016/j.marpol.2014.04.006, 2014.

Madureira, P., Brekke, H., Cherkashov, G., and Rovere, M.: Exploration of polymetallic nodules in the Area: Reporting practices, data management and transparency, Mar. Pol., 70, 101–107, doi:10.1016/j.marpol.2016.04.051, 2016.

Martínez Arbizu, P., and Haeckel, M.: RV SONNE Fahrtbericht / Cruise Report SO239: EcoResponse Assessing the Ecology, Connectivity and Resilience of Polymetallic Nodule Field Systems, Balboa (Panama) – Manzanillo (Mexico,) 11.03.-30.04.2015 (Report No. doi:10.3289/GEOMAR_REP_NS_25_2015), GEOMAR Helmholtz-Zentrum für Ozeanforschung, Kiel, Germany, 2015.
Menendez, A., James, R. H., Lichtschlag, A., Connelly, D. and Peel, K.: Controls on the chemical composition on ferromanganese nodules in the Clarion-Clipperton Fracture Zone, eastern equatorial Pacific, Mar. Geol., 409, 1-14, 2018.
Menot, L., and Rühlemann, C., and BIONOD Shipboard party: BIONOD Cruise Science Report, Vol. 2 French Licence Area, Ifremer, REM/EEP/LEP13.06, 57p, 2013.
Mero, J. L.: The Mineral Resources of the Sea, Elsevier, Amsterdam, 1965.
Mewes, K., Mogollón, J. M., Picard, A., Rühlemann, C., Eisenhauer, A., Kuhn, T., Ziebis, W., and Kasten, S.: Diffusive transfer of oxygen from seamount basaltic crust into overlying sediments: An example from the Clarion–Clipperton Fracture Zone, Earth Planet. Sci. Lett., 433, 215–225, doi:10.1016/j.epsl.2015.10.028, 2016.
Mewes, K., Mogollón, J. M., Picard, A., Rühlemann, C., Kuhn, T., Nöthen, K., and Kasten, S.: Impact of depositional and biogeochemical processes on small scale variations in nodule abundance in the Clarion-Clipperton Fracture Zone, Deep-Sea Res. Part I: Oceanogr. Res. Pap., 91, 125–141, doi:10.1016/j.dsr.2014.06.001, 2014.
Miljutin, D. M., Miljutina, M. A., Martínez Arbizu, P., and Galeron, J.: Deep-sea nematode assemblage has not recovered 26 years after experimental mining of polymetallic nodules (CCFZ, Pacific), Deep-Sea Res. Part I: Oceanogr. Res. Pap., 58, 885–897, 2011.
Mogollón, J. M., Mewes, K., and Kasten, S.: Quantifying manganese and nitrogen cycle coupling in manganese-rich, organic carbon-starved marine sediments: Examples from the Clarion-Clipperton fracture zone, Geophys. Res. Lett., 43, 2016GL069117, doi:10.1002/2016GL069117, 2016.
Morgan, C. L., Nichols, J. A., Selk, B. W., Toth, J. R., and Wallin, C.: Preliminary analysis of exploration data from Pacific deposits of manganese nodules, Mar. Georesour. Geotechnol., 11, 1-25, 1993.
Müller, P. J., Hartmann, M., and Suess, E.: The chemical environment of pelagic sediments, in: The Manganese Nodule Belt of the Pacific Ocean: Geological Environment, Nodule Formation, and Mining Aspects, edited by Halbach, P., Friedrich, G., and von Stackelberg, U., Enke, Stuttgart, pp. 70-90, 1988.
Müller, P. J., and Mangini, A.: Organic carbon decomposition rates in sediments of the pacific manganese nodule belt dated by 230Th and 231Pa, Earth Planet. Sci. Lett., 51, 94-114, 1980.
Nöthen, K., and Kasten, S.: Reconstructing changes in seep activity by means of pore water and solid phase Sr/Ca and Mg/Ca ratios in pockmark sediments of the Northern Congo Fan, Mar. Geol., 287, 1–13, doi:10.1016/j.margeo.2011.06.008, 2011.
Oebius, H. U., Becker, H. J., Rolinski, S., and Jankowski, J. A.: Parametrization and evaluation of marine environmental impacts produced by deep-sea manganese nodule mining, Deep-Sea Res. Part II Top. Stud. Oceanogr., 48, 3453–3467, doi:10.1016/S0967-0645(01)00052-2, 2001.
Paul, S. A. L., Gaye, B., Haeckel, M., Kasten, S., and Koschinsky, A.: Biogeochemical Regeneration of a Nodule Mining Disturbance Site: Trace Metals, DOC and Amino Acids in Deep-Sea Sediments and Pore Waters, Front. Mar. Sci., 5, doi: 10.3389/fmars.2018.00117, 2018.
Pearson, K.: Notes on regression and inheritance in the case of two parents, Proc. Royal Soc. London, 58, 240–242, 1895.
Purser, A., Marcon, Y., Hoving, H.-J. T., Vecchione, M., Piatkowski, U., Eason, D., Bluhm, H., and Boetius, A.: Association of deep-sea incirrate octopods with manganese crusts and

nodule fields in the Pacific Ocean, Curr. Biol., 26, R1268–R1269, doi:10.1016/j.cub.2016.10.052, 2016, 2016.
Radziejewska, T.: Response of deep-sea meiobenthic communities to sediment disturbance simulating effects of polymetallic nodule mining, Int. Rev. Hydrobiol., 87, 457-477, 2002.
Ramirez-Llodra E., Tyler P. A., Baker M. C., Bergstad O. A., Clark M. R., Escobar, E., Levin, L. A., Menot, L., Rowden, A. A., Smith, C. R., and Van Dover, C. L.: Man and the Last Great Wilderness: Human Impact on the Deep Sea, PLoS ONE, 6, e22588, doi:10.1371/journal.pone.0022588, 2011.
Redfield, A. C.: On the proportions of organic derivations in sea water and their relation to the composition of plankton, in: James Johnstone Memorial Volume, edited by Daniel, R. J., University Press of Liverpool, pp. 176–192, 1934.
Rühlemann, C., Kuhn, T., Wiedicke, M., Kasten, S., Mewes, K., and Picard, A.: Current status of manganese nodule exploration in the German license area, Proceedings of the Ninth (2011) ISOPE Ocean Mining Symposium, Maui, Hawaii, USA, June 19-24, 2011, 168-173, 2011.
Rühlemann, C., Albers, L., Briand, P., Brulport, J.-P., Cosson, R., Dekov, V. M., Galéron, J., Goergens, R., Gueguen, B., Hansen, J., Kaiser, S., Kefel, O., Khripounoff, A., Kuhn, T., Larsen, K., Menot, L., Mewes, K., Miljutin, D., Mohrbeck, I., Nealova, L., Perret-Gentil, L., Regocheva, A., Wegorzewski, A., and Zoch, D., BIONOD Cruise report, p. 299, 2012.
Scott, S. D.: Seafloor Polymetallic Sulfides: Scientific Curiosities or Mines of the Future? In: Marine Minerals, edited by: Teleki, P. G., Dobson, M. R., Moore, J. R., and von Stackelberg, U., NATO ASI Series (Series C: Mathematical and Physical Sciences), 194, Springer, Dordrecht, 1987.
Sharma, R.: Indian Deep-sea Environment Experiment (INDEX):: An appraisal. Deep-Sea Res. Part II Top. Stud. Oceanogr., 48, 3295-3307, doi:10.1016/S0967-0645(01)00041-8, 2001.
Smith, C. R., Levin, L. A., Koslow, A., Tyler, P. A., and Glover, A. G.: The near future of the deep seafloor ecosystems, in: Aquatic Ecosystems: Trends and Global Prospects, edited by Polunin, N. V. C., Cambridge University Press, 334–353, doi: 10.1017/CBO9780511751790.030, 2008.
Smith, K. L., White, G. A., and Laver, M. B.: Oxygen uptake and nutrient exchange of sediments measured in situ using a free vehicle grab respirometer. Deep Sea Res. Part II, 26, 337-346, doi:10.1016/0198-0149(79)90030-X, 1979.
Soetaert, K., and Meysman, F.: Reactive transport in aquatic ecosystems: Rapid model prototyping in the open source software R, Environ. Model. Softw., 32, 49–60, doi:10.1016/j.envsoft.2011.08.011, 2012.
Spickermann, R.: Rare Earth Content of Manganese Nodules in the Lockheed Martin Clarion-Clipperton Zone Exploration Areas, Proc. Off. Technol. Conf., Houston Texas, 2012.
Stratmann, T., Lins, L., Purser, A., Marcon, Y., Rodrigues, C. F., Ravara, A., Cunha, M. R., Simon-Lledó, E., Jones, D. O. B., Sweetman, A. K., Köser, K., and van Oevelen, D.: Abyssal plain faunal carbon flows remain depressed 26 years after a simulated deep-sea mining disturbance, Biogeosciences, 15, 4131-4145, doi.org/10.5194/bg-15-4131-2018, 2018.
Thiel, H., and Forschungsverband Tiefsee-Umweltschutz: Evaluation of the environmental consequences of polymetallic nodule mining based on the results of the TUSCH Research Association, Deep-Sea Res. Part II Top. Stud. Oceanogr., 48, 3433-3452, doi:10.1016/S0967-0645(01)00051-0, 2001.
Trueblood, D. D., and Ozturgut, E.: The benthic impact experiment: A study of the ecological impacts of deep seabed mining on abyssal benthic communities, Proc. of the 7th ISOPE Conference, Honolulu, Hawaii, 1997.
Van Dover, C. L.: Tighten regulations on deep-sea mining, Nature, 470, 31-33, doi: 10.1038/470031a, 2011.

Vanreusel, A., Hilario, A., Ribeiro, P. A., Menot, L., and Arbizu, P. M.: Threatened by mining, polymetallic nodules are required to preserve abyssal epifauna, Sci. Rep., 6, 26808, doi:10.1038/srep26808, 2016.

Volz, J. B., Liu, B., Köster, M., Henkel, S., Koschinsky, A., and Kasten, S.: Post-depositional manganese mobilization during the last glacial period in sediments of the eastern Clarion-Clipperton Zone, Pacific Ocean, Earth Planet. Sci. Lett., 532, 116012, doi:10.1016/j.epsl.2019.116012, 2020.

Volz, J. B, Mogollón, J. M., Geibert, W., Martínez Arbizu, P., Koschinsky, A., Kasten, S.: Natural spatial variability of depositional conditions, biogeochemical processes and element fluxes in sediments of the eastern Clarion-Clipperton Zone, Pacific Ocean, Deep-Sea Res. Part I, 140, 159-172, 2018.

Wedding, L. M., Reiter, S. M., Smith, C. R., Gjerde, K. M., Kittinger, J. N., Friedlander, A. M., Gaines, S. D., Clark, M. R., Thurnherr, A. M., Hardy, S. M., and Crowder, L. B.: Managing mining of the deep seabed, Science, 349, 144-145, 2015.

Widmann, P.: Enrichment of mobilizable manganese in relation to manganese nodules abundance, Master thesis, Eberhard Karls Universität Tübingen and the Federal Institute for Geoscience and Resources, Hannover, 182 p., 2015.

Ziebis, W., McManus, J., Ferdelman, T., Schmidt-Schierhorn, F., Bach, W., Muratli, J., Edwards, K. J., and Villinger, H.: Interstitial fluid chemistry of sediments underlying the North Atlantic gyre and the influence of subsurface fluid flow, Earth Planet. Sci. Lett., 323–324, 79–91, doi:10.1016/j.epsl.2012.01.018, 2012.

Zonneveld, K., Versteegh, G., Kasten, S., Eglinton, T. I., Emeis, K.-C., Huguet, C., Koch, B. P., de Lange, G. J., de Leeuw, J. W., Middelburg, J. J., Mollenhauer, G., Prahl, F., Rethemeyer, J. and Wakeham, S.: Selective preservation of organic matter in marine environments; processes and impact on the sedimentary record, Biogeosciences, 7, 483-511, 2010.

Figure captions

Figure 1: Sampling sites (black circles, black star) in various European contract areas for the exploration of manganese nodules within the Clarion-Clipperton Fracture Zone (CCZ). Investigated stations are located in the German BGR area (blue), eastern European IOM area (yellow), Belgian GSR area (green) and French IFREMER area (red). The two stations within the German BGR area are located in the "prospective area" (BGR-PA, black star) and in the "reference area" (BGR-RA, black circle). The contract areas granted/governed by the International Seabed Authority (ISA; white areas) are surrounded by nine Areas of Particular Environmental Interest (APEI), which are excluded from any mining activities (green shaded squares). Geographical data provided by the ISA.

Figure 2: Examples of undisturbed reference sediments in the German BGR-PA area and the French IFREMER area and pictures of small-scale disturbances for the simulation of deep-sea mining within the CCZ, which are investigated in the framework of this study (years: yr; months: mth; days: d). Copyright: ROV KIEL 6000 Team, GEOMAR Helmholtz Centre for Ocean Research Kiel, Germany.

Figure 3: Solid-phase Mn and TOC contents for all disturbed sites investigated in the framework of this study.

Figure 4: Correlation of solid-phase Mn and TOC contents between the disturbed sites and the respective undisturbed reference sediments (grey shaded profiles) using the disturbance depths determined with the Pearson correlation coefficient (compare Table 3). For the undisturbed reference sediments, solid-phase Mn contents are taken from Volz et al. (2020) and TOC contents are taken from Volz et al. (2018).

Figure 5: Model results of the transient transport-reaction model for (a) the EBS disturbance in the German BGR-RA area and (b) the IOM-BIE disturbance in the eastern European IOM area. The model is adapted after the steady state transport-reaction model presented in Volz et al. (2018) and shows the response of the geochemical system in the sediments if steady state conditions are disturbed by the removal of the upper 10 cm (BGR-RA, average disturbance depth of BGR-PA and BGR-RA; cf. Table 3) and 7 cm (IOM; Table 3) of the sediments while maintaining the same boundary conditions but with reduced bioturbation over the first 100 years after the disturbance.

Figure 6: Detailed model results of the transient transport-reaction model (Figure 5) for the upper 1 m of the sediments with the fit of the simulated profiles with the analytical data for undisturbed sediments at current steady state geochemical conditions and for the new steady state geochemical system after the disturbance (dark blue profiles) for (a) EBS disturbance in the German BGR-RA area and (b) the IOM-BIE disturbance in the eastern European IOM area.

Figure 7: Pore-water fluxes of oxygen (O_2), nitrate (NO_3^{2-}) and ammonia (NH_4^+) at the sediment-water interface obtained by the application of the transient transport-reaction model. Oxygen fluxes into the sediment and fluxes of nitrate and ammonia towards the sediment surface are shown as a function of time after the EBS and IOM-BIE disturbances in the German BGR-RA area (blue) and in the eastern European IOM area (black), respectively.

Figure 8: Conceptual model for time-dependent pore-water fluxes of oxygen (O_2), nitrate (NO_3^{2-}) and ammonia (NH_4^+) at the sediment-water interface after the removal of the upper 7-10 cm of the sediments. The re-establishment of bioturbation, the maximum oxygen penetration depth (OPD) as well as the re-establishment of the surface sediment layer dominated by the reactive labile organic matter fraction are indicated as a function of time after the sediment removal.

Table captions

Table 1: MUC and PC cores investigated in this study including information on geographic position, water depth, type and age of the disturbances (years: yr; months: mth; days: d).

Table 2: Information of sedimentation rate (Sed. rate), flux of particulate organic carbon (POC) to the seafloor, bioturbation depth (Bioturb. depth), oxygen penetration depth (OPD) based on GC cores from the investigated sites and determined in the study by Volz et al. (2018). Information for the BGR-PA area is taken from an adjacent site (A5-2-SN; 11°57.22'N, 117°0.42'W) studied by Mewes et al. (2014) and Mogollón et al. (2016).

Table 3: Calculated Pearson correlation coefficients r_{Mn} and r_{TOC} for the determination of the disturbance depth of various small-scale disturbances investigated in the framework of this study (compare Table 1). For both correlations, the highest positive linear Pearson coefficient for solid-phase Mn contents ($r_{\mathrm{Mn}} \sim 1$) between the disturbed sites and the respective undisturbed reference sites was used.

Figure 1:

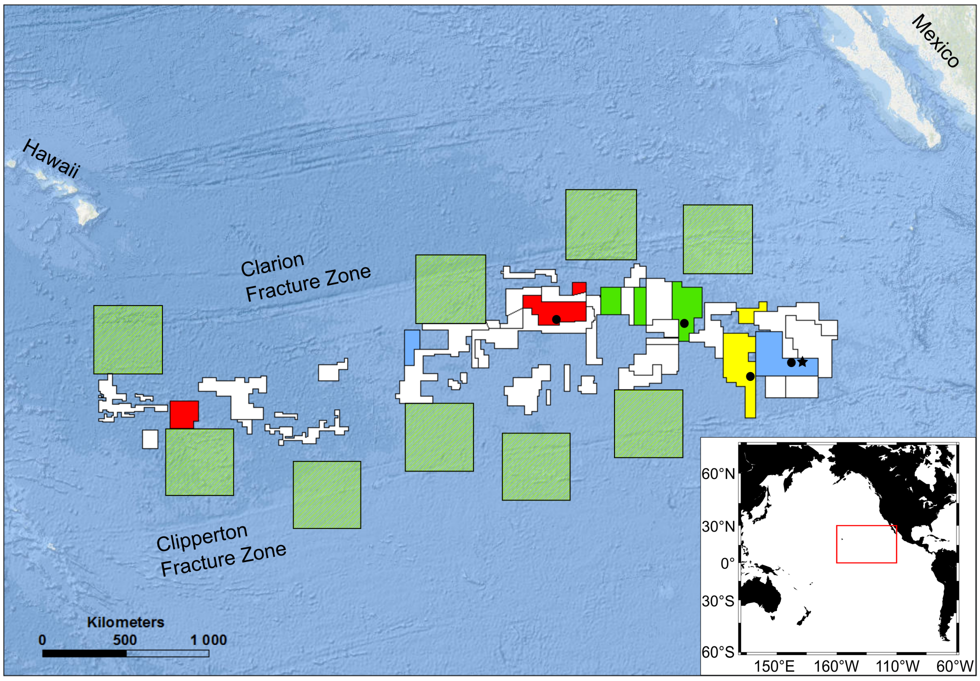

Mexico
Hawaii
Clarion
Fracture Zone
Clipperton
Fracture Zone
Kilometers
0
500
1 000
60°N
30°N
0°
30°S
60°S
150°E
160°W
110°W
60°W

Figure 2:

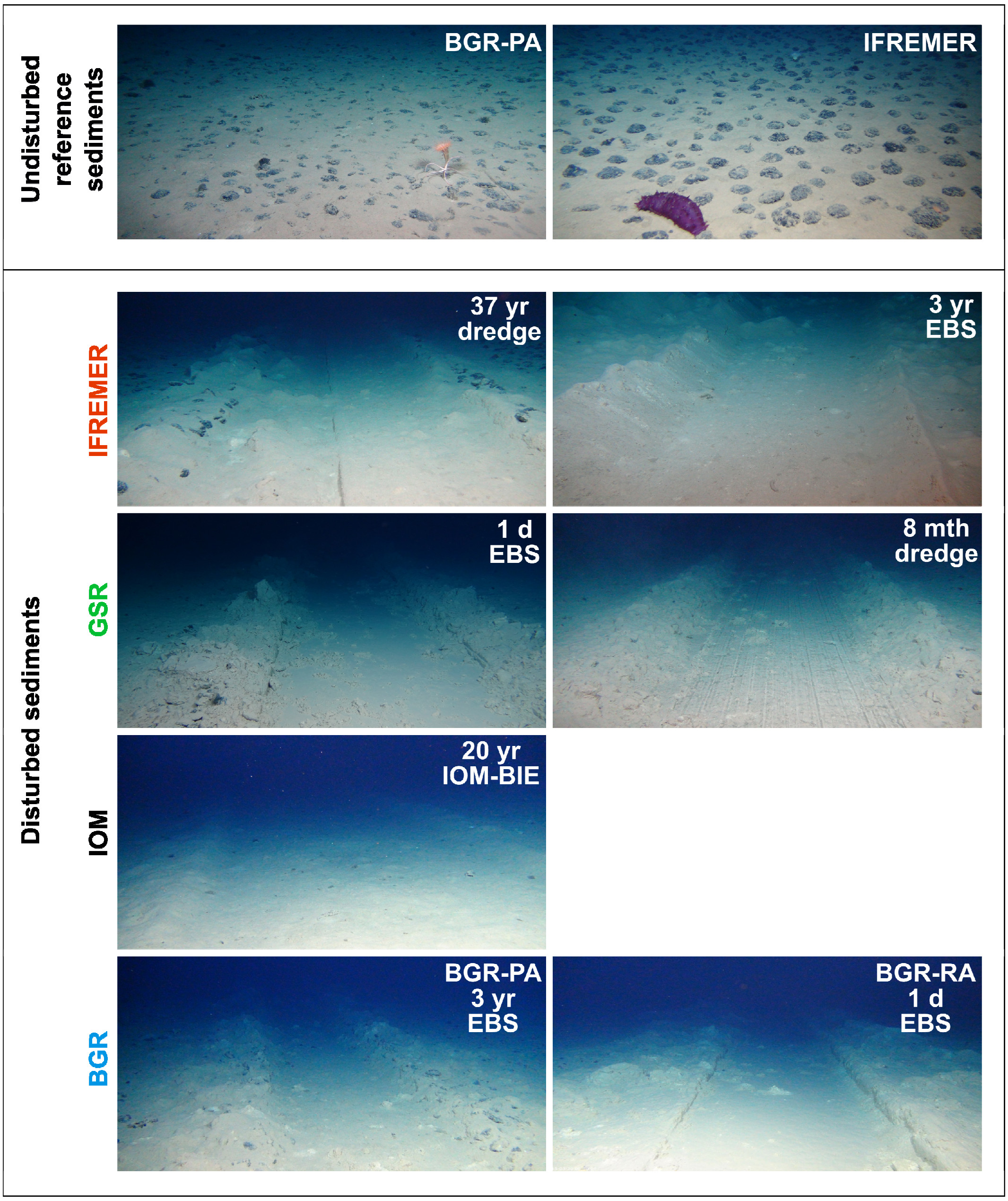
Undisturbed reference sediments
BGR-PA
IFREMER
Disturbed sediments
IFREMER
37 yr dredge
3 yr EBS
GSR
1 d EBS
8 mth dredge
IOM
20 yr IOM-BIE
BGR
BGR-PA 3 yr EBS
BGR-RA 1 d EBS

Figure 3:

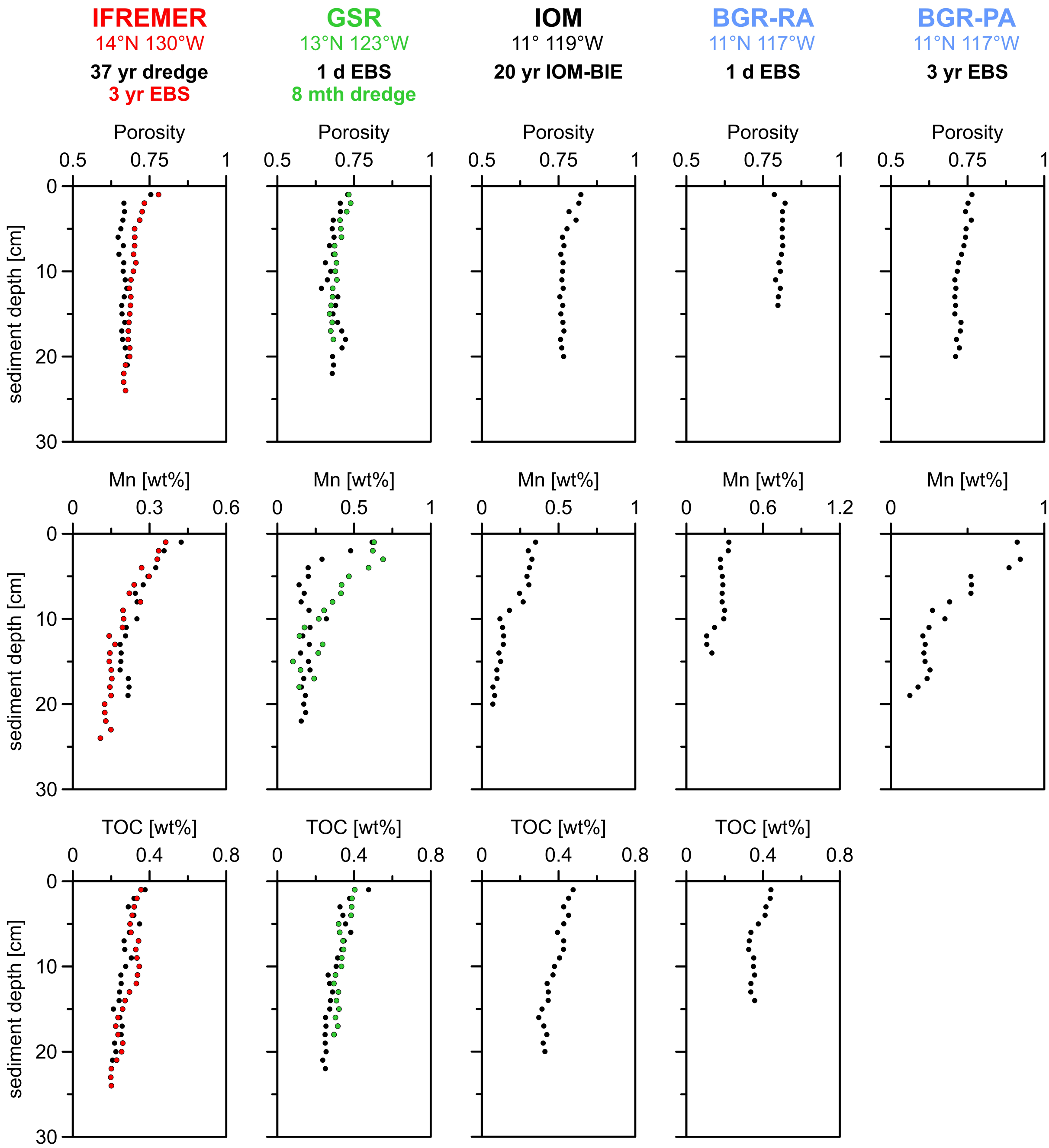
IFREMER
14°N 130°W
37 yr dredge
3 yr EBS
GSR
13°N 123°W
1 d EBS
8 mth dredge
IOM
11° 119°W
20 yr IOM-BIE
BGR-RA
11°N 117°W
1 d EBS
BGR-PA
11°N 117°W
3 yr EBS
Porosity
0.5
0.75
1
Mn [wt%]
0
0.3
0.6
0.5
0.6
1.2
TOC [wt%]
0.4
0.8
sediment depth [cm]
0
10
20
30

Figure 4:

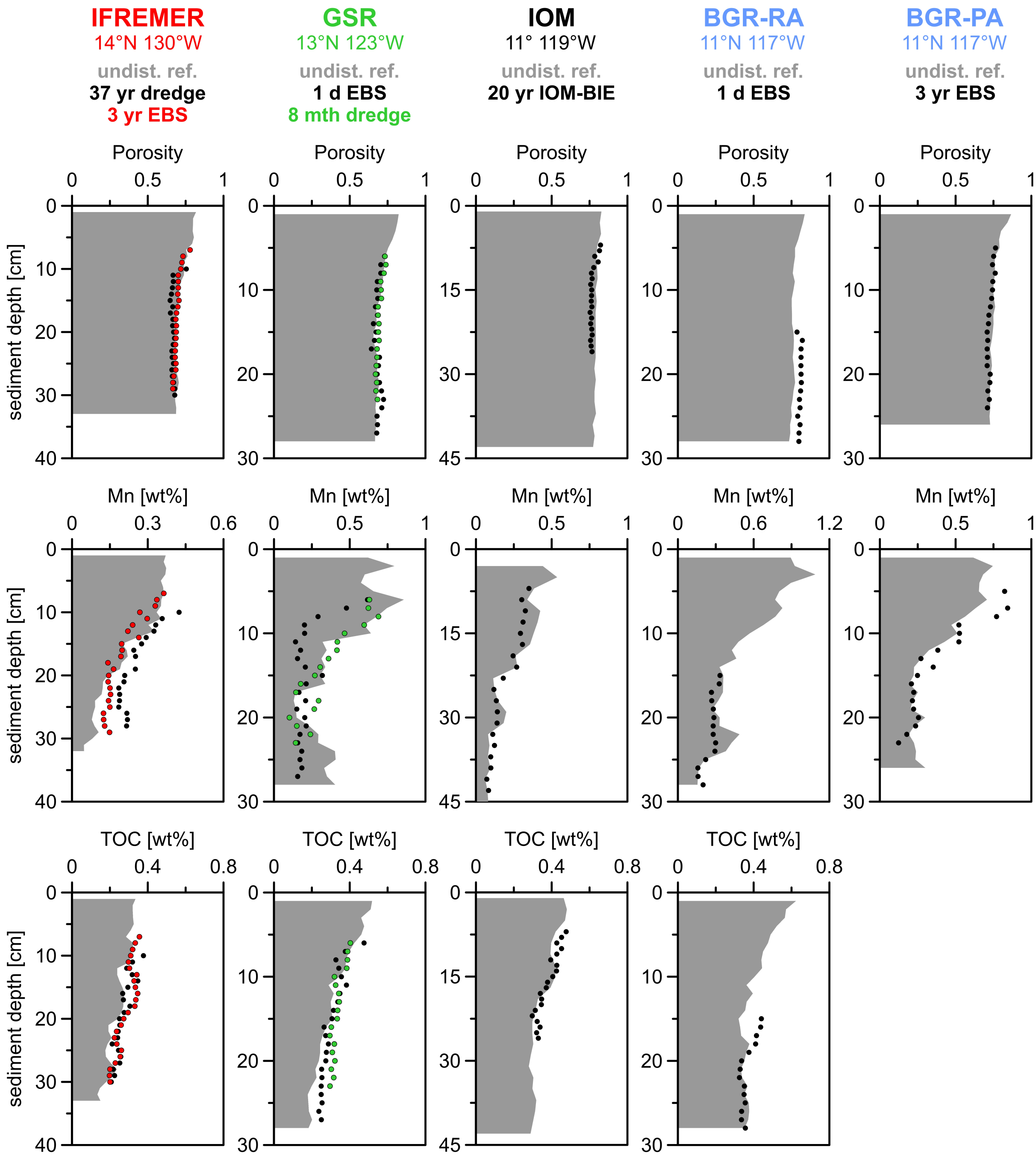

IFREMER
14°N 130°W
undist. ref.
37 yr dredge
3 yr EBS
GSR
13°N 123°W
undist. ref.
1 d EBS
8 mth dredge
IOM
11° 119°W
undist. ref.
20 yr IOM-BIE
BGR-RA
11°N 117°W
undist. ref.
1 d EBS
BGR-PA
11°N 117°W
undist. ref.
3 yr EBS
Porosity
Mn [wt%]
TOC [wt%]
sediment depth [cm]

Figure 5:

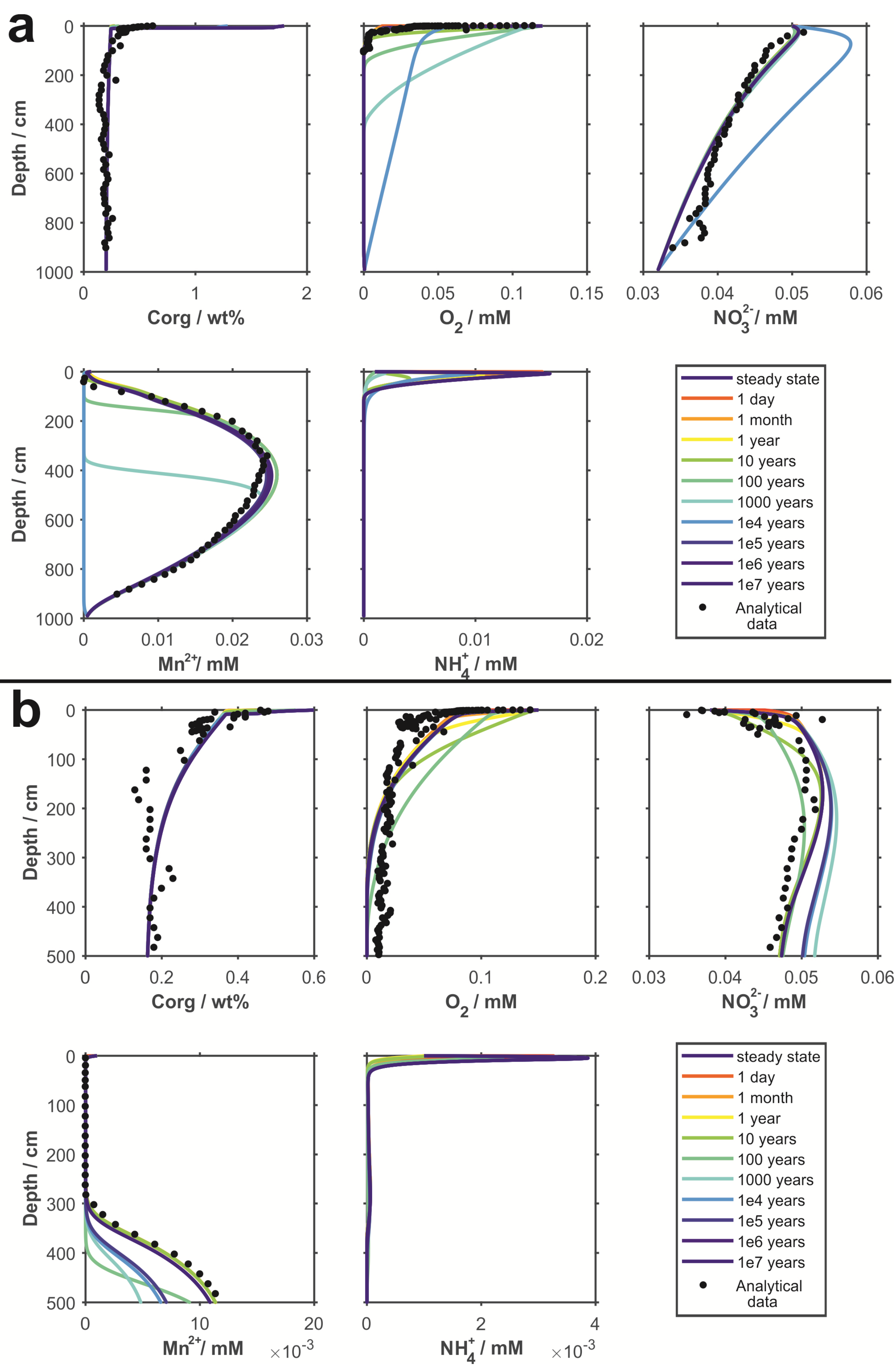

a
b
Depth / cm
Corg / wt%
O_2 / mM
NO_3^{2-} / mM
Mn^{2+}/ mM
NH_4^+ / mM
$\times10^{-3}$
steady state
1 day
1 month
1 year
10 years
100 years
1000 years
1e4 years
1e5 years
1e6 years
1e7 years
Analytical data

Figure 6:

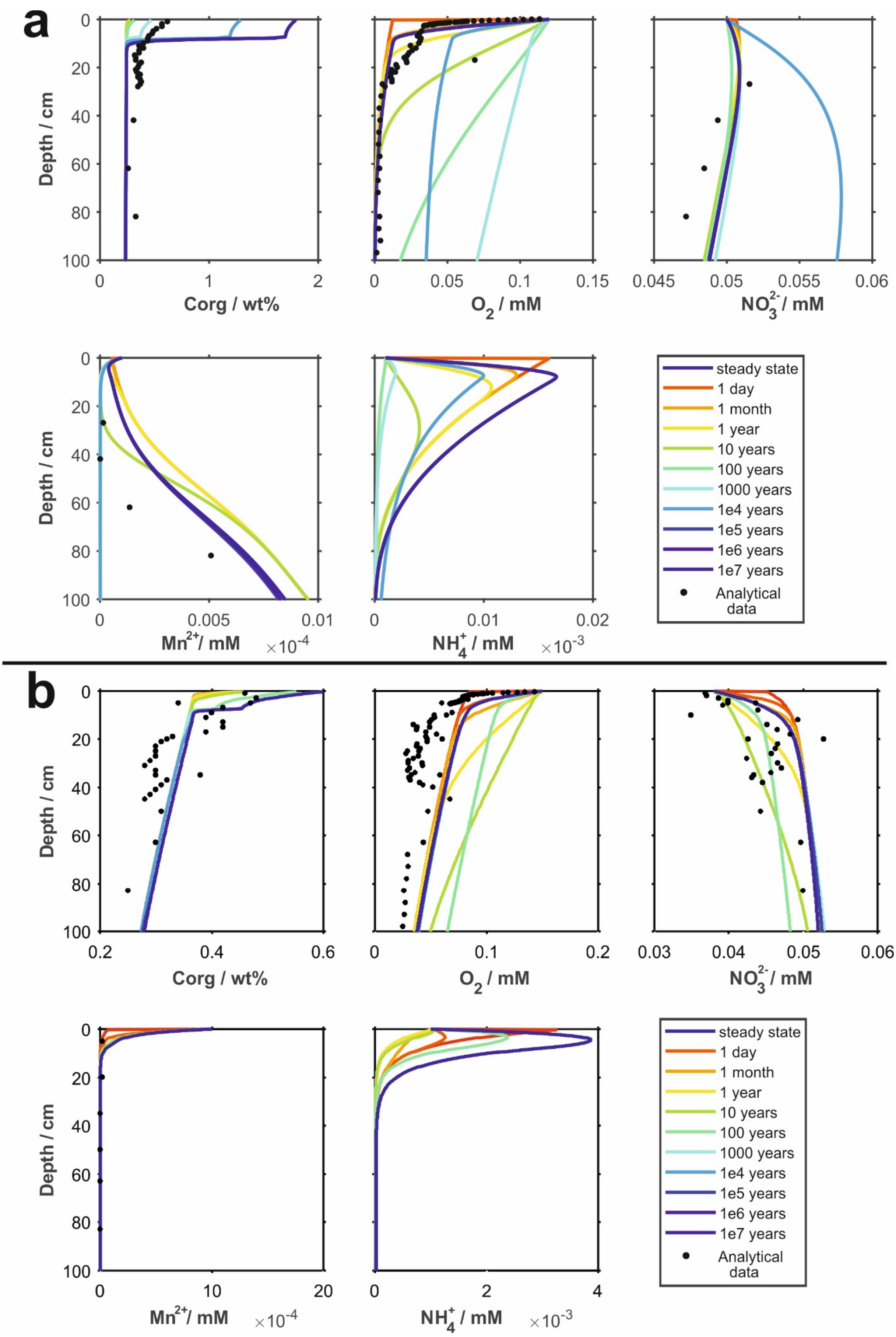

a
Depth / cm
Corg / wt%
O2 / mM
NO3 2- / mM
Mn2+/ mM ×10-4
NH4+ / mM ×10-3
steady state
1 day
1 month
1 year
10 years
100 years
1000 years
1e4 years
1e5 years
1e6 years
1e7 years
Analytical data
b
Depth / cm
Corg / wt%
O2 / mM
NO3 2- / mM
Mn2+/ mM ×10-4
NH4+ / mM ×10-3
steady state
1 day
1 month
1 year
10 years
100 years
1000 years
1e4 years
1e5 years
1e6 years
1e7 years
Analytical data

Figure 7:

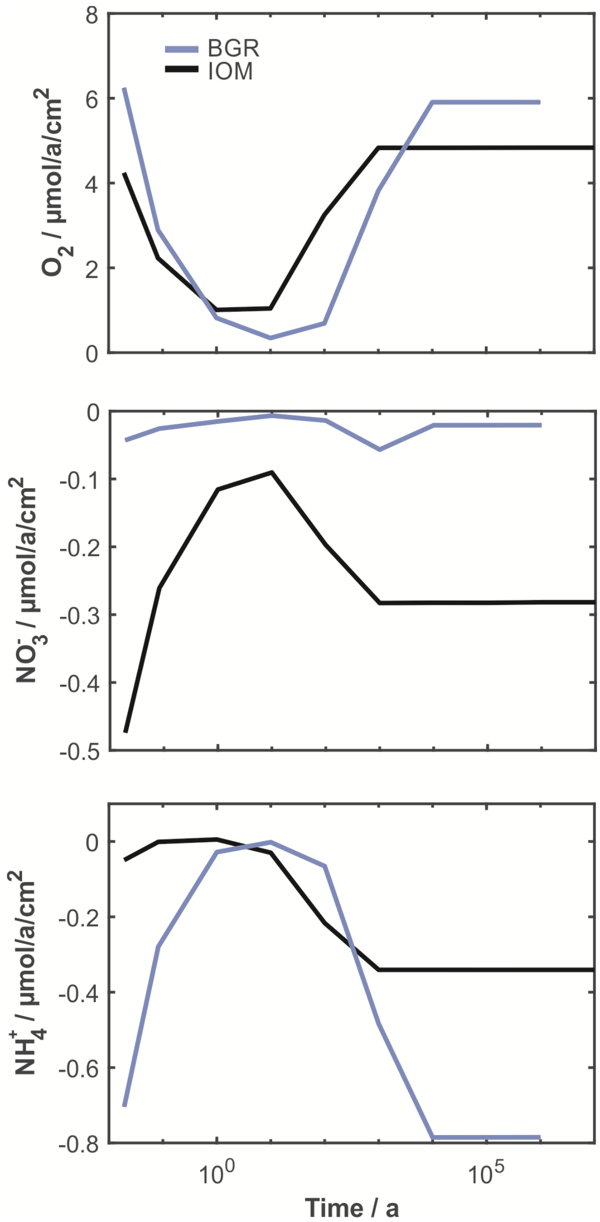
BGR
IOM
O2 / µmol/a/cm2
NO3- / µmol/a/cm2
NH4+ / µmol/a/cm2
8
6
4
2
0
-0.1
-0.2
-0.3
-0.4
-0.5
-0.6
-0.8
10^0
10^5
Time / a

Figure 8:

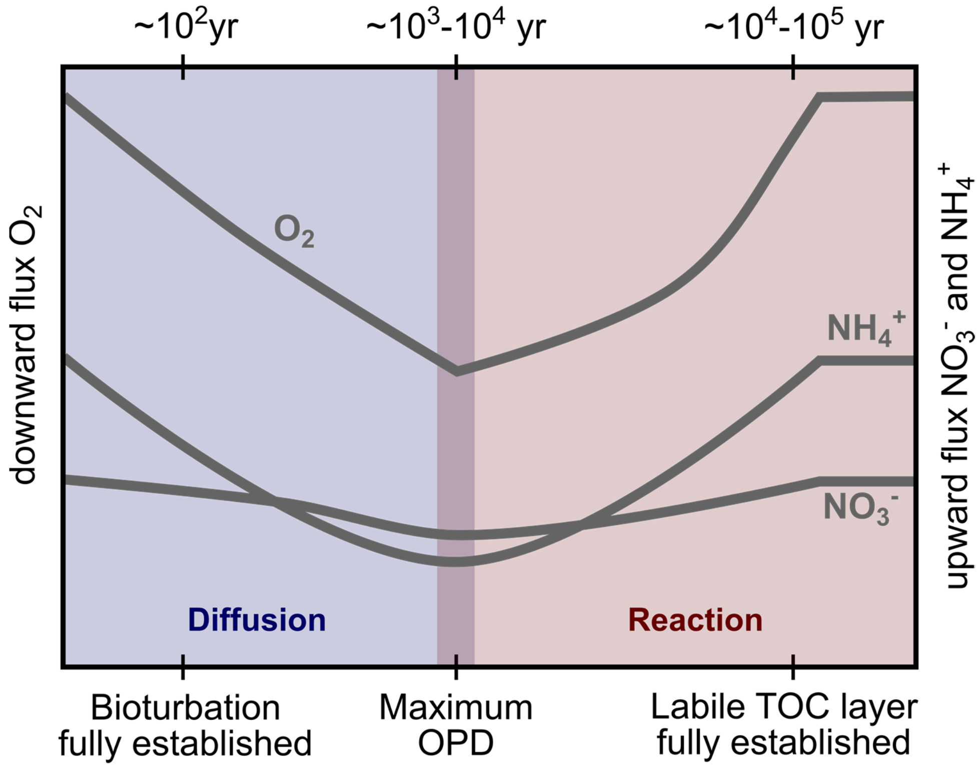

~10²yr
~10³-10⁴ yr
~10⁴-10⁵ yr
downward flux O₂
upward flux NO₃⁻ and NH₄⁺
O₂
NH₄⁺
NO₃⁻
Diffusion
Reaction
Bioturbation fully established
Maximum OPD
Labile TOC layer fully established

Table 1:

Area	Site	Coring device	Disturbance device/type	Disturbance age	Latitude [N]	Longitude [W]	Water depth [m]
BGR-PA	39	MUC	-	-	11°50.64'	117°03.44'	4132.0
BGR-PA	41	PC	EBS[1]	3 yr	11°50.92'	117°03.77'	4099.2
BGR-RA	62	GC	-	-	11°49.12’	117°33.22’	4312.2
BGR-RA	64	PC	EBS[2]	1 d	11°48.27'	117°30.18'	4332
BGR-RA	66	MUC	-	-	11°49.13'	117°33.13'	4314.8
IOM	84	MUC	-	-	11°04.73'	119°39.48'	4430.8
IOM	87	GC	-	-	11°04.54’	119°39.83’	4436
IOM	101	PC	IOM-BIE[3]	20 yr	11°04.38'	119°39.38'	4387.4
GSR	121	MUC	-	-	13°51.25'	123°15.3'	4517.7
GSR	131	PC	EBS[2]	1 d	13°52.38'	123°15.1'	4477.6
GSR	141	PC	dredge[4]	8 mth	13°51.95'	123°15.33'	4477
IFREMER	157	PC	dredge[5]	37 yr	14°02.06'	130°07.23'	4944.5
IFREMER	161	PC	EBS[1]	3 yr	14°02.20'	130°05.87'	4999.1
IFREMER	175	MUC	-	-	14°02.45'	130°05.11'	5005.5

[1]Epibenthic sledge (EBS) during BIONOD cruises in 2012 onboard L’Atalante (Brenke, 2005; Rühlemann and Menot, 2012; Menot and Rühlemann, 2013)
[2]Epibenthic sledge (EBS) during RV SONNE cruise SO239 in 2015 (Brenke, 2005; Martínez Arbizu and Haeckel, 2015)
[3]Benthic impact experiment (BIE); disturbance created with the Deep-Sea Sediment Re-suspension System (DSSRS; e.g., Brocket and Richards, 1994; Kotlinski et al., 1998)
[4]Towed dredge sampling during GSR cruise in 2014 onboard M.V. Mt Mitchell (Jones et al., 2017)
[5]Towed dredge sampling by the Ocean Minerals Company (OMCO) in 1978 onboard Hughes Glomar Explorer (Morgan et al., 1993; Spickermann, 2012)

Table 2:

Area	Sed. rate [cm kyr^{-1}]	POC flux [mg C_{org} m^{-2} d^{-1}]	Bioturb. depth [cm]	OPD [m]
BGR-PA	~0.53[a]	~6.9[a]	~5[a]	~2[a,b]
BGR-RA	0.65	1.99	7	0.5
IOM	1.15	1.54	13	3
GSR	0.21	1.51	8	>7.4
IFRE-1	0.64	1.47	7	4.5
IFRE-2	0.48	1.5	8	3.8
APEI3	0.2	1.07	6	>5.7

[a]Mogollón et al. (2016)
[b]Mewes et al. (2014)

Table 3:

Exploration area	Disturbance device/type	Disturbed Site	Reference Site	r_{Mn}	Disturbance depth [cm]	r_{TOC}
BGR-PA	EBS	41	39	0.86	5	-
BGR-RA	EBS	64	66	0.82	15	-0.4
IOM	IOM-BIE	101	87	0.97	7	0.77
GSR	EBS	131	121	0.72	6	0.88
GSR	dredge	141	121	0.88	6	0.91
IFREMER	dredge	157	175	0.74	10	0.73
IFREMER	EBS	161	175	0.93	7	0.74